Title
Three-Dimensional Boron Cluster Pharmacophores

Author
Saebi, Azin

Publication Date
2017

Peer reviewed|Thesis/dissertation

UNIVERSITY OF CALIFORNIA

Los Angeles

Three-Dimensional Boron Cluster Pharmacophores

A thesis submitted in partial satisfaction

of the requirements for the degree Master of Science

in Biochemistry, Molecular and Structural Biology

by

Azin Saebi

2017

ABSTRACT OF THE THESIS

Three-Dimensional Boron Cluster Pharmacophores

by

Azin Saebi

Master of Science in Biochemistry, Molecular and Structural Biology

University of California, Los Angeles, 2017

Professor Alexander Michael Spokoyny, Chair

Carbon-rich aromatic molecules have been historically utilized as major building blocks for assembly of complex molecular architectures due to the vast development of methods for fine-tuning their properties. Yet, the classical toolbox of 2D aromatic building blocks presents inherent topological limitations, which sometimes is referred to as “molecular flatland”. Boron clusters introduce potentially a powerful solution for addressing this limitation by offering an inherently rigid, three-dimensional scaffold available for dense functionalization. In biological systems, this dense functionalization can be exploited to enhance specific interactions with protein surfaces. In this thesis, the application of boron clusters as novel pharmacophores has been investigated in two cases: 1) development of rigid and atomically precise nanomolecules and 2) development of isoform-specific and blood-brain barrier permeable histone deacetylase inhibitors.

The thesis of Azin Saebi is approved.

Richard B. Kaner

Pamela J. Kennedy

Alexander Michael Spokoyny, Committee Chair

University of California, Los Angeles

2017

TABLE OF CONTENTS

LIST OF ACRONYMS

LC-MS	Liquid chromatography-mass spectrometry
TIC	Total ion chromatogram
NMR	Nuclear magnetic resonance
TLC	Thin layer chromatography
UV	Ultra violet
R_f	Retention factor
DI water	Deionized water
DCM	Dichloromethane
MeOH	Methanol
EtOH	Ethanol
THF	Tetrahydrofuran
^{i}PrOH	Isopropyl alcohol
ACN	Acetonitrile
Et_2O	Diethyl ether
DCE	Dichloroethane
TFA	Trifluoroacetic acid
STAB-H	Sodium triacetoxyborohydride
AcOH	Acetic acid
DMSO-d	Deuterated dimethyl sulfoxide

ACKNOWLEDGMENTS

First, I would like to sincerely thank my advisor, Professor Alexander M. Spokoyny, for introducing me to the world of boron cluster chemistry and providing me the opportunity to grow as a scientist. I am beyond grateful for his exceptional mentorship, guidance, and continuous support over the past two years. I am also incredibly grateful to the entire Spokoyny group, especially my mentors Dr. Jonathan C. Axtell, Rafal M. Dziedzic, and Elaine A. Qian, whose insight, encouragement, and endless hours of training made this thesis possible. Furthermore, I would like to thank Elamar Hakim Moully, Marry A. Waddington, and Farinaz Ghodrati for their help and motivation over the past few years. Finally, I am grateful to my family for their endless love and support, and for inspiring me to pursue my dreams.

I would like to thank the UCLA CARE/MSD scholars program for supporting me for during this work (under grant number GM055052), I am specifically grateful to Dr. Tama Hasson for her guidance and encouragement.

The first chapter of this thesis is adapted from the previously published work.[I]

[I] Qian, E. A., Wixtrom, A. I., Axtell, J. C., Saebi, A., Jung, D., Rehak, P., Han, Y., Moully, E. H., Mosallaei, D., Chow, S., Messina, M., Wang, J.-Y., Royappa, A. T., Rheingold, A. L., Maynard, H. D., Kral, P., and Spokoyny, A. M. *Nature Chem.*, **2017**, 9, 333-340. doi:10.1038/nchem.2686.

Chapter 1: Development of Atomically Precise Organomimetic Cluster Nanomolecules

1. 1. Introduction

Signal transduction is integral to the communication between cells and the extracellular environment. The majority of signals are initiated and propagated through binding events between proteins, and can involve multiple specific interactions between their surfaces. Such multivalent interactions are important because they boost the binding strength and furthermore result in efficient signal transduction with high fidelity.[1,2]

Due to the important functions multivalency serves in nature, chemists have been interested in exploiting multivalency for the synthesis of protein-binding ligands. These pharmaceutical ligands are designed to incorporate multivalency in order to promote both the binding and selectivity toward their target. A well-studied example of a multivalent synthetic system is gold nanoparticles (AuNPs) capped with thiolated ligands.[3,4] AuNPs are able to display ligands with tunable density on their surfaces, exploiting multivalency for target recognition. Moreover, the AuNPs are easily synthesized and are often biocompatible, which are desirable characteristics for applications within the biological systems.[5] Nonetheless, the gold-thiolate bond is weak (40-50 kcal mol^{-1}) and quite susceptible to thiol-ligand desorption and exchange in solution.[3,6,7] Therefore, AuNPs lack the atomic precision needed to study biological systems.[8,9]

We set out to address this issue through the development of atomically precise hybrid nanomolecules that feature robust molecular structure, such that the composition remains fully well-defined in biological systems (**Figure 1-1**). The proposed nanomolecules feature three main components: 1) a rigid and stable inorganic cluster as the core of nanomolecule, 2) thiolated ligands densely packed on the surface and 3) perfluoroaromatic "linker" moieties, covalently connecting the ligands to the core. We chose to utilize the *closo*-dodecaborate cluster as the core structure –

this robust scaffold exhibits convex icosahedral geometry with the 12 vertices occupied by boron atoms.[10-12] This cluster can be perfunctionalized such that each vertex is covalently attached to the linker.[13-15] On the other side of the linker, a perfluoroaryl ring is displayed, which in the presence of thiolated ligands and an appropriate base, can undergo efficient 'click'-like nucleophilic aromatic substitution (S_NAr) chemistry under mild conditions. The product is a fully covalent organomimetic cluster nanomolecule (OCN) displaying 12 copies of the ligand on its surface. Due to the facile nature of the S_NAr chemistry, assembly of OCNs is comparable to that of AuNPs in terms of synthetic ease.[16-19] Furthermore, a wide scope of thiols (small molecules, sugars, polymers, peptides) have been used to assemble the OCNs, indicating high tolerance for other functional groups.

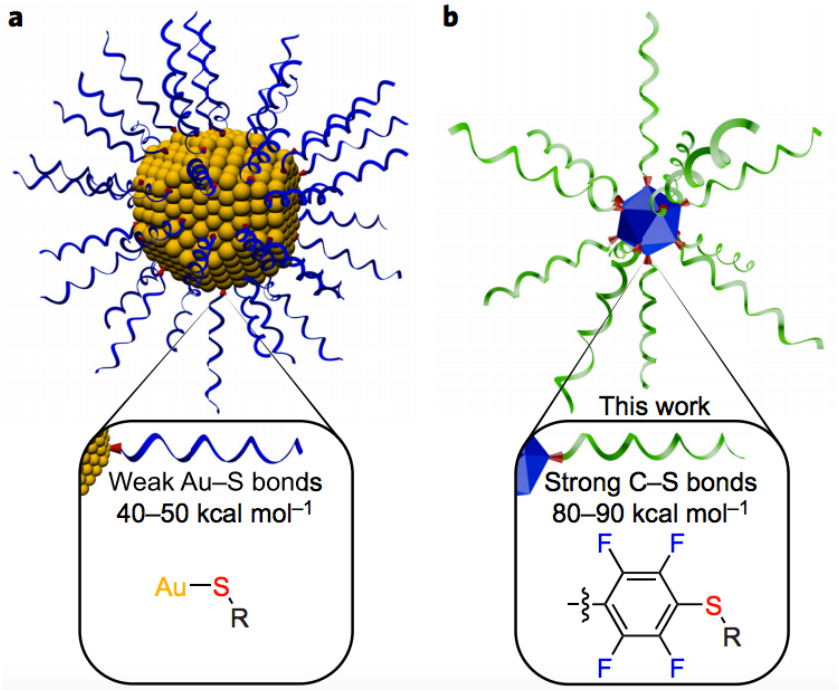

Figure 1-1. Comparison of AuNPs with OCNs. Panel **a** depicts schematic of a gold nanoparticle coated with thiolated ligands. Panel **b** is the schematic of the proposed OCNs, constructed with fully covalent linkages.

One of the most attractive features of AuNPs is their size tunability. In contrast to AuNPs, the OCNs have an inherently defined core that cannot be adjusted in size. Thus, the key to tuning the size of OCNs lies in the design of the linker molecule. The simplest linker consists of a single pentafluoroaromatic ring (G1 linker, **Figure 1-2a**). However, the linker can be rationally extended by the addition of a second aromatic group, operating as a spacer, giving rise to the G2 linker (**Figure 1-2b**). We have shown that OCNs can be assembled with either the G1 or G2 linkers (**Figure 1-3**).

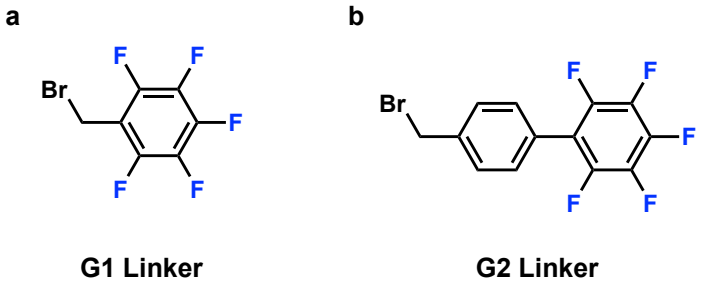

Figure 1-2. G1 and G2 linkers both feature a perfluoroaromatic ring to facilitate S_NAr chemistry.

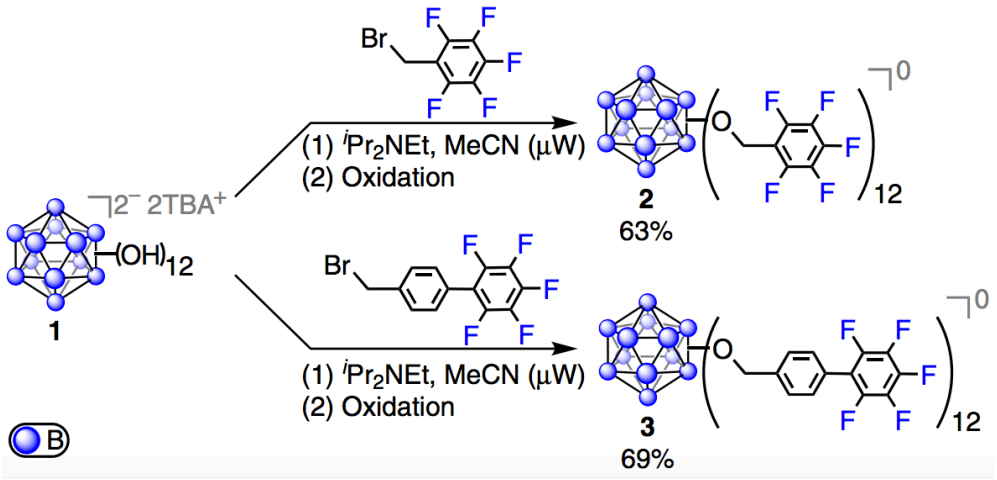

Figure 1-3. OCNs can be synthesized with either G1 or G2 linkers, leading to synthesis of G1 and G2 OCNs respectively.

As confirmed by single crystal X-ray diffraction, the addition of the second aromatic ring increases the particle size from 1.9 nm with G1 linker to 2.7 nm with G2 linker, while retaining the rigidity of the resulting OCN (**Figure 1-4**). In this thesis, I will describe the synthesis of the G2 linker molecule. Furthermore, I will also describe the synthesis of a polymeric ligand, thiolated methoxypoly(ethylene glycol) (mPEG-SH). mPEG-SH is utilized in synthesis of PEGylated OCNs, which are highly hydrophilic and stable in biologically-relevant media.

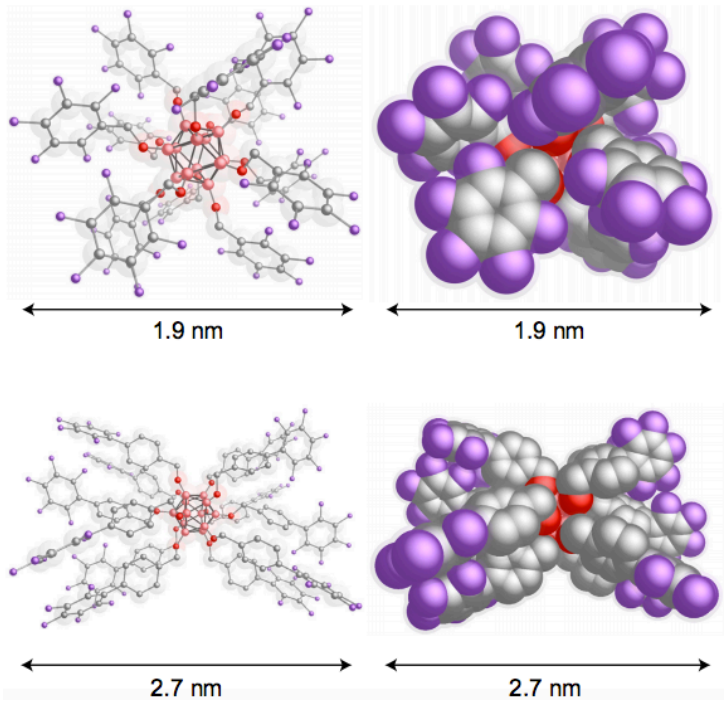

Figure 1-4. Crystal X-ray diffraction results confirms the size tunability of OCNs. OCNs constructed with G1 linker are 1.9 nm, whereas the OCNs with G2 clusters are 2.7 nm. Ball-and-stick representations of the single-crystal X-ray structures are depicted on left and the space-filling representations are on right.

1. 2. Methods

1. 2. 1. Synthesis of G2 Linker

General Considerations

The G2 linker was synthesized through the reaction scheme depicted in **Figure 1-5**. The 4-pentafluorophenyl benzaldehyde (starting material) was synthesized.

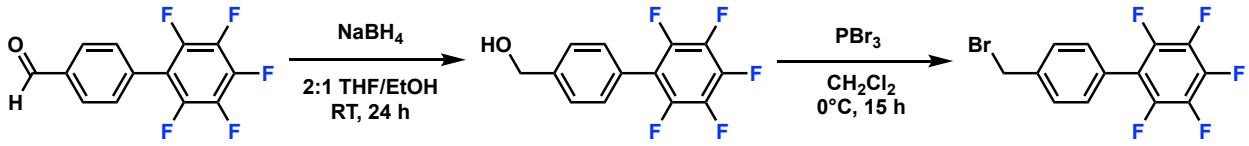

Figure 1-5. The scheme for synthesis of the G2 linker.

Synthesis of 4-pentafluorophenyl (hydroxymethyl) benzene

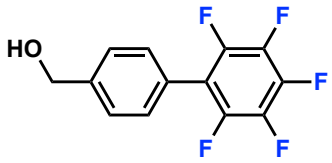

A solution of 4-pentafluorophenyl benzaldehyde (0.900 g, 3.30 mmol) and sodium borohydride (0.150 g, 3.96 mmol) in 14 mL tetrahydrofuran and 7 mL ethanol was prepared and placed under a positive nitrogen flow. The mixture was stirred at room temperature for 24 hours. The resulting dark solution was diluted with water (30 mL) and extracted with methylene chloride (30 mL). The organic layer was washed three times with H_2O, dried over $MgSO_4$, and filtered through Celite. The solvent was then dried *in vacuo*. The residue was purified by flash chromatography (eluent: DCM; $R_f = 0.4$) through a silica column, using UV light for TLC visualization. The resulting solution was dried under vacuum, providing 4-pentafluorophenyl (hydroxymethyl) benzene as a white solid (0.705 g, 78%).

Synthesis of 4-pentafluorophenyl (bromomethyl) benzene

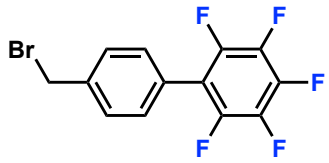

A flask containing 4-pentafluorophenyl (hydroxymethyl) benzene (1.00 g, 3.65 mmol) was purged with nitrogen and 30 mL of dry methylene chloride was charged into the flask. The solution was placed in ice bath and PBr_3 (346 μL, 3.65 mmol) was added with a syringe. Reaction mixture was stirred overnight (15 hours), turning into a yellow color. The resulting mixture was then diluted with 100 mL distilled H_2O. The organic layer was separated and washed 3 times with saturated NaCl solution. Organic layer was collected and dried over $MgSO_4$, then filtered through Celite. Solvent was evaporated and the residue was purified by flash chromatography (hexane/DCM, 2:1; R_f = 0.75) through a silica column, using UV light for TLC visualization. The resulting solution was dried under vacuum, providing 4-pentafluorophenyl (bromomethyl) benzene as a white solid (0.773 g, 63%).

1. 2. 2. Synthesis of mPEG-thiol Ligand

General Considerations

The mPEG-thiol was synthesized through the reaction scheme depicted in **Figure 1-6**. The starting material, $mPEG_{750}$ with average molecular weight of 750 Da, was purchased from Acros Organics and used without further purifications.

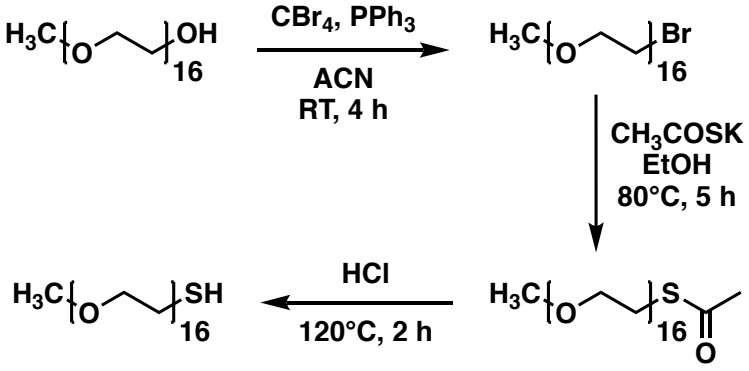

Figure 1-6. The scheme for synthesis of the G2 linker.

Synthesis of mPEG-Br

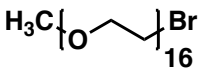

In a round bottom flask, $mPEG_{750}$ (7.50 g, 10.00 mmol) and CBr_4 (3.98 g, 12.00 mmol) were dissolved in 40 mL of acetonitrile. To the stirring solution, PPh_3 (3.15 g, 6.00 mmol) was added in small portions over 30 minutes. The mixture was then left stirring at room temperature. After 4 hours, the solvent was removed *in vacuo* and the resulting yellow-orange oil was dissolved in 20 mL of H_2O and left at 4° C overnight, producing a white precipitate. The mixture was filtered through Celite* on a glass frit and the filtrate was washed twice with 5 mL of toluene. The aqueous layer was dried *in vacuo* to yield the desired product (7.08 g, 87%).

*Celite was pretreated on the frit by washing with 30 mL of H_2O before the mixture was filtered.

Synthesis of mPEG-SAc

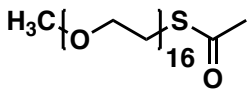

To a solution of mPEG-Br (1.07 g, 1.32 mmol) in 35 mL of ethanol, potassium thioacetate (0.20 g, 1.75 mmol) was added in one portion. The mixture was refluxed at 120°C for 5 hours. The resulting suspension was filtered through Celite and the filtrate was dried under vacuum, affording a brown oil. The oil was dissolved in 40 mL of chloroform and the organic phase was washed twice with H_2O. The organic layer was dried over Na_2SO_4 and filtered through Celite. The solvent was removed *in vacuo*, providing mPEG-SAc (0.64 g, 74%).

Synthesis of mPEG-SH

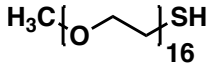

mPEG-SAc (405 mg, 0.5 mmol) was charged with 5 mL of 1M HCl and was refluxed at 110°C for 2 hours. The solvent was removed *in vacuo*. The residue was dissolved in 10 mL of DCM and the organic phase was washed twice with water. The organic layer was separated and dried over Na_2SO_4 and filtered through Celite. The solution was dried under vacuum to yield mPEG-SH (319 mg, 83%). Product was stored under inert atmosphere.

1. 3. Results

1. 3. 1. Characterization of G2 Linker

The 4-pentafluorophenyl (hydroxymethyl) benzene was characterized by ^{1}H (**Figure 1-7**), ^{13}C (**Figure 1-8**), and ^{19}F (**Figure 1-9**) NMR spectroscopy. Similarly, 4-pentafluorophenyl (bromomethyl) benzene was characterized by ^{1}H (**Figure 1-10**), ^{13}C (**Figure 1-11**), and ^{19}F (**Figure 1-12**) NMR spectroscopy. The results indicate successful synthesis and purification of the products.

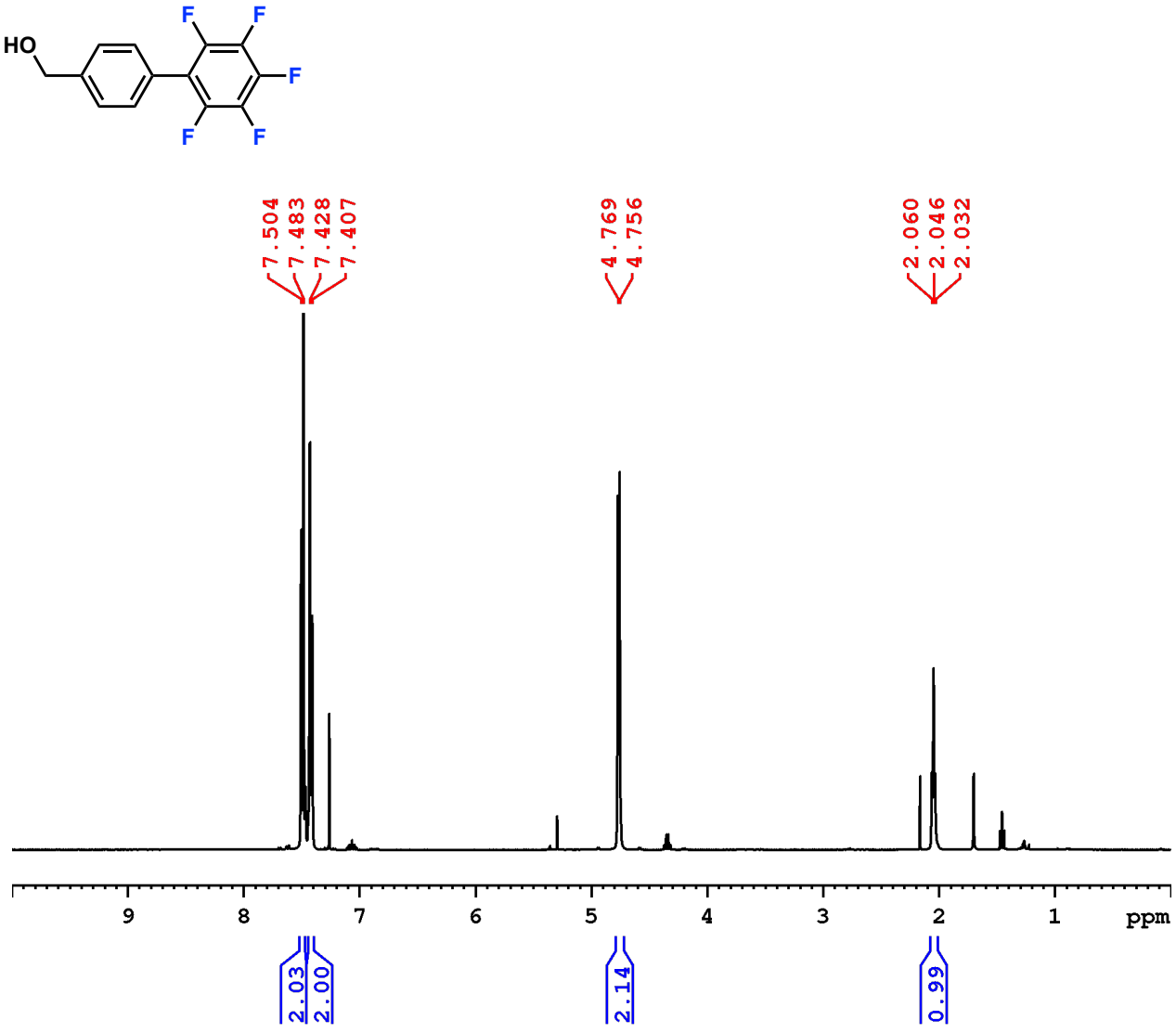

Figure 1-7. ^{1}H NMR spectrum of 4-pentafluorophenyl (hydroxymethyl) benzene in $CDCl_3$.

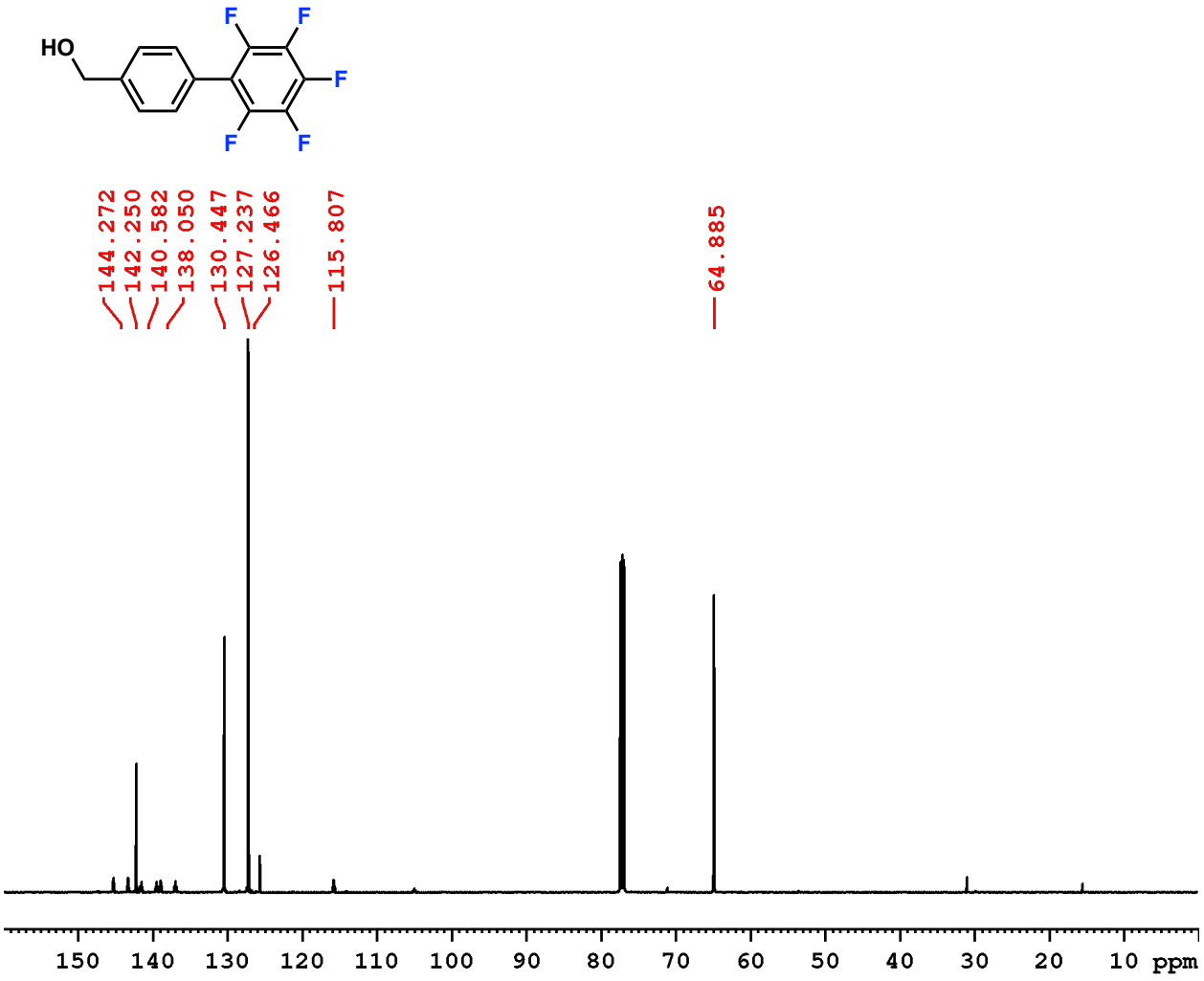

Figure 1-8. $^{13}C\{^{1}H\}$ NMR spectrum of 4-pentafluorophenyl (hydroxymethyl) benzene in $CDCl_3$.

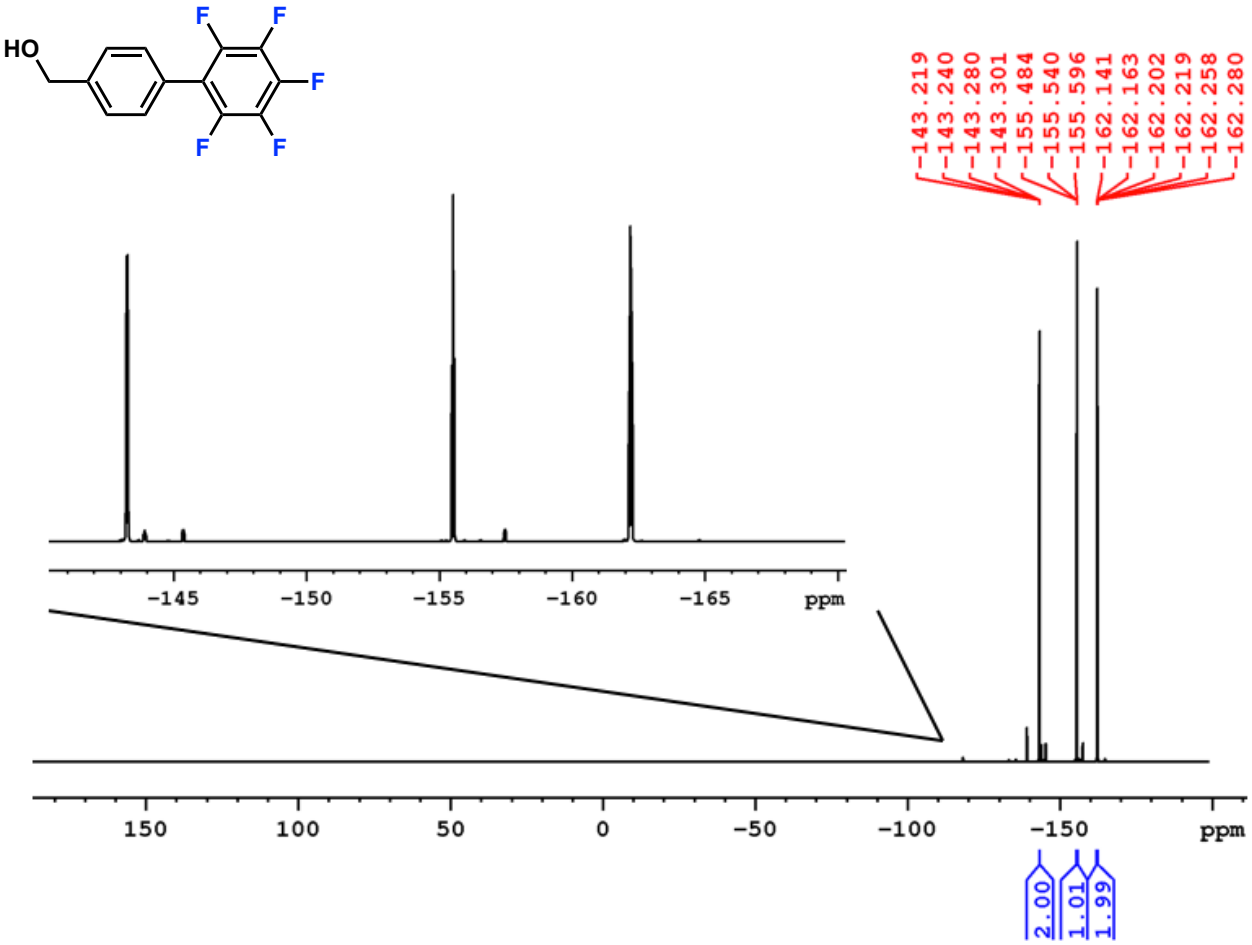

Figure 1-9. ^{19}F NMR spectrum of 4-pentafluorophenyl (hydroxymethyl) benzene in $CDCl_3$.

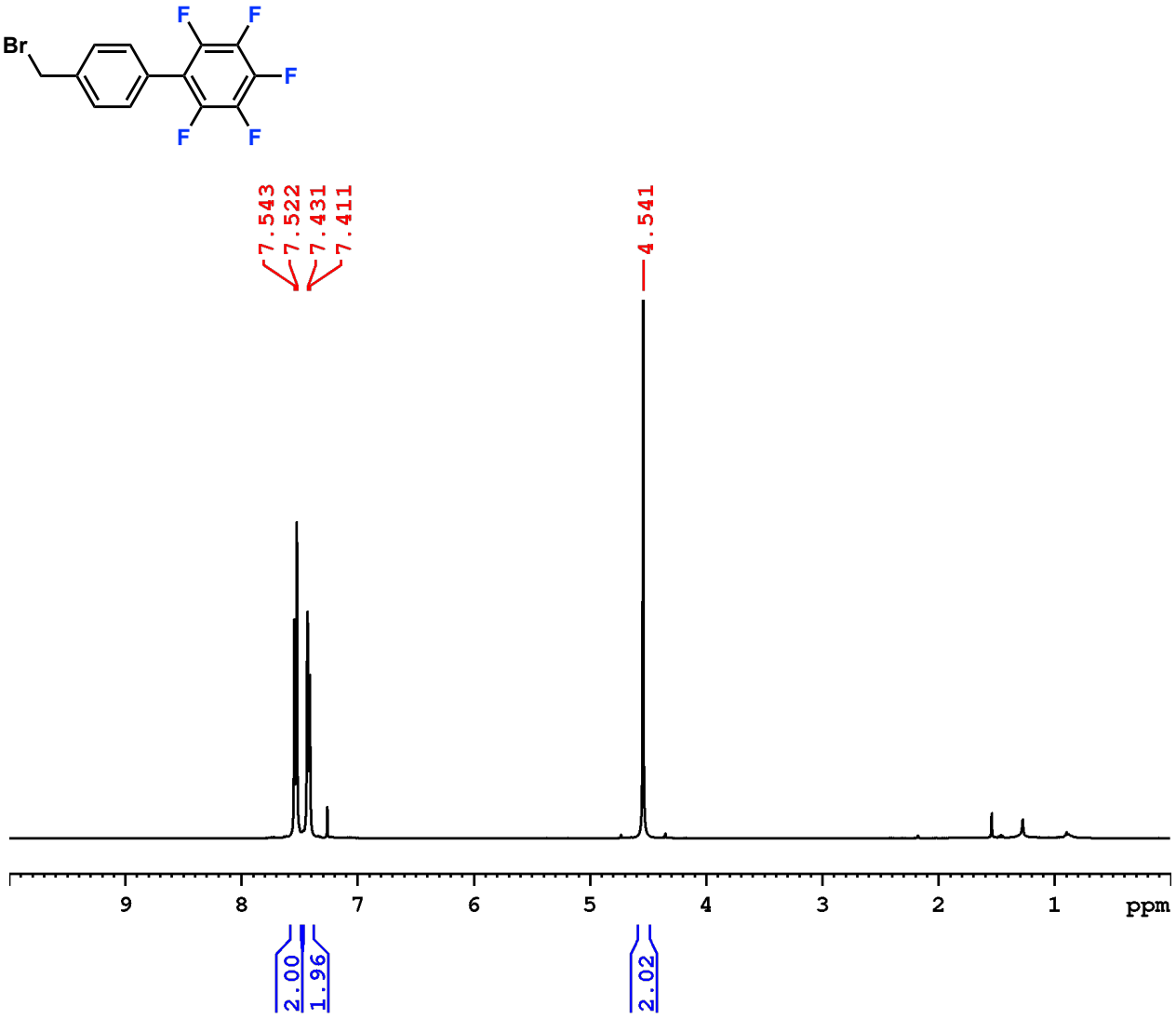

Figure 1-10. ^{1}H NMR spectrum of 4-pentafluorophenyl (bromomethyl) benzene in $CDCl_3$.

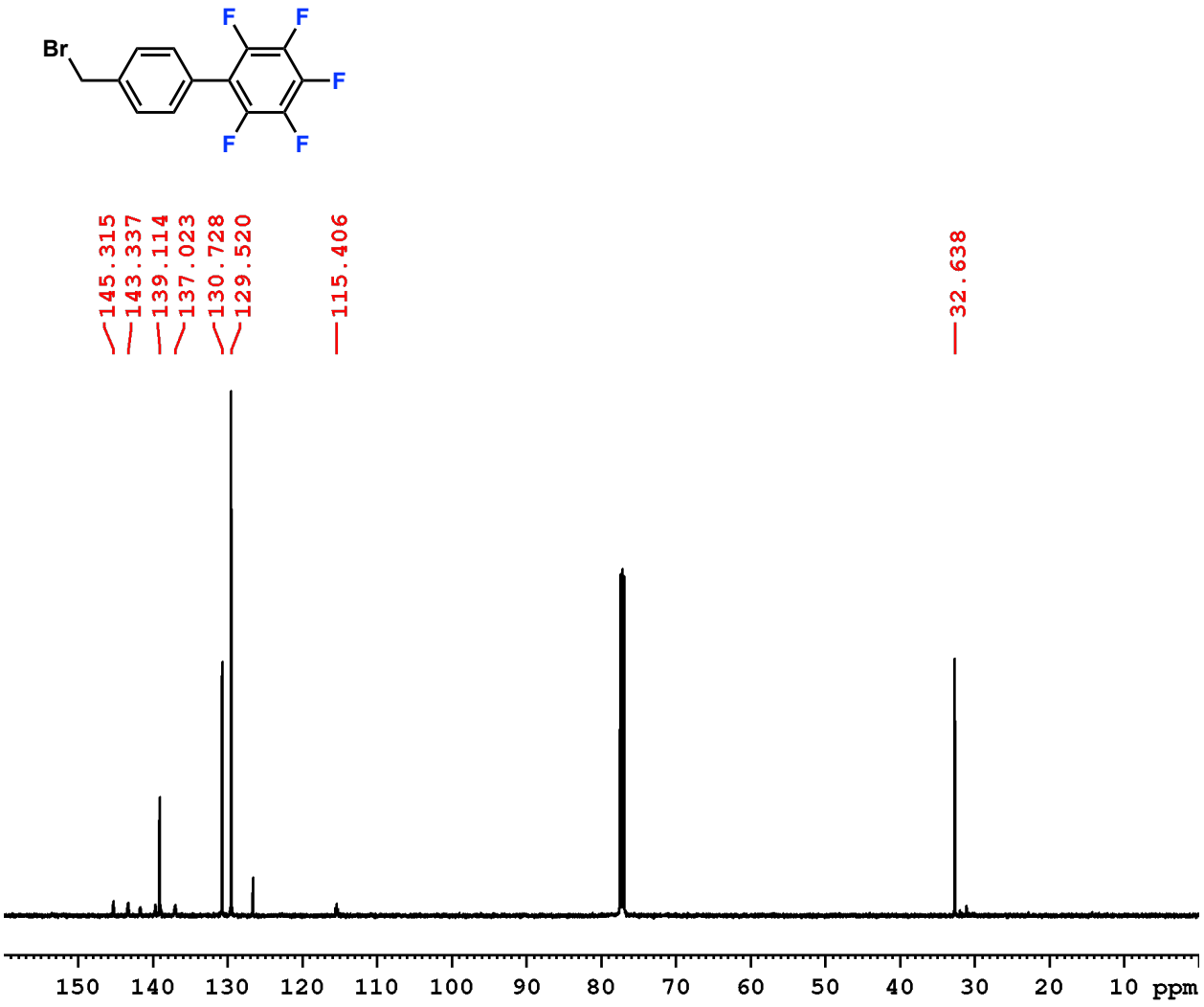

Figure 1-11. $^{13}C\{^{1}H\}$ NMR spectrum of 4-pentafluorophenyl (bromomethyl) benzene in $CDCl_3$.

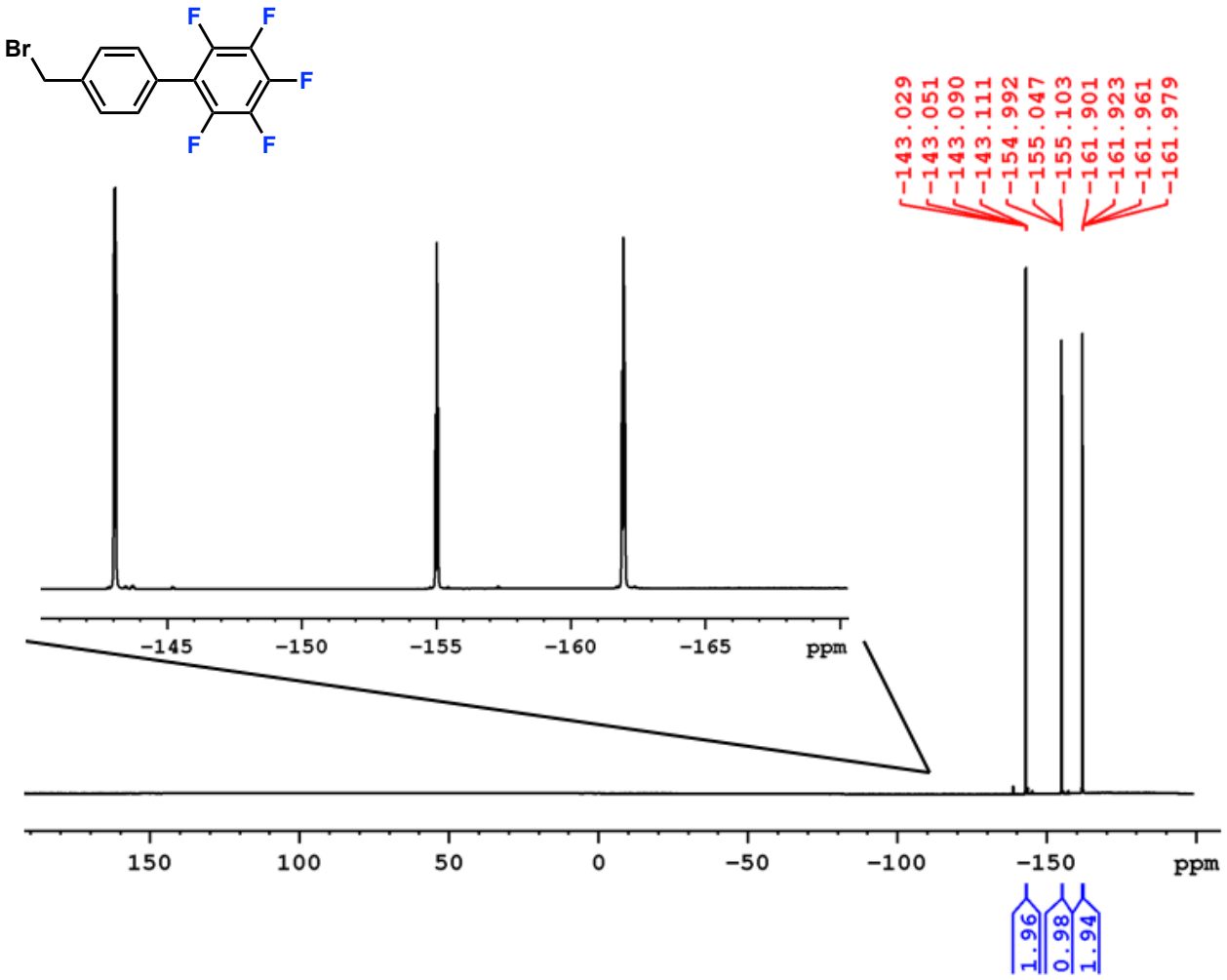

Figure 1-12. ^{19}F NMR spectrum of 4-pentafluorophenyl (bromomethyl) benzene in $CDCl_3$.

1. 3. 2. Characterization of mPEG-thiol Ligand

All intermediates were characterized by ^{1}H NMR spectroscopy. The spectra of mPEG-Br, mPEG-SAc, and mPEG-SH are presented in **Figure 1-13**, **Figure 1-14**, and **Figure 1-15** respectively.

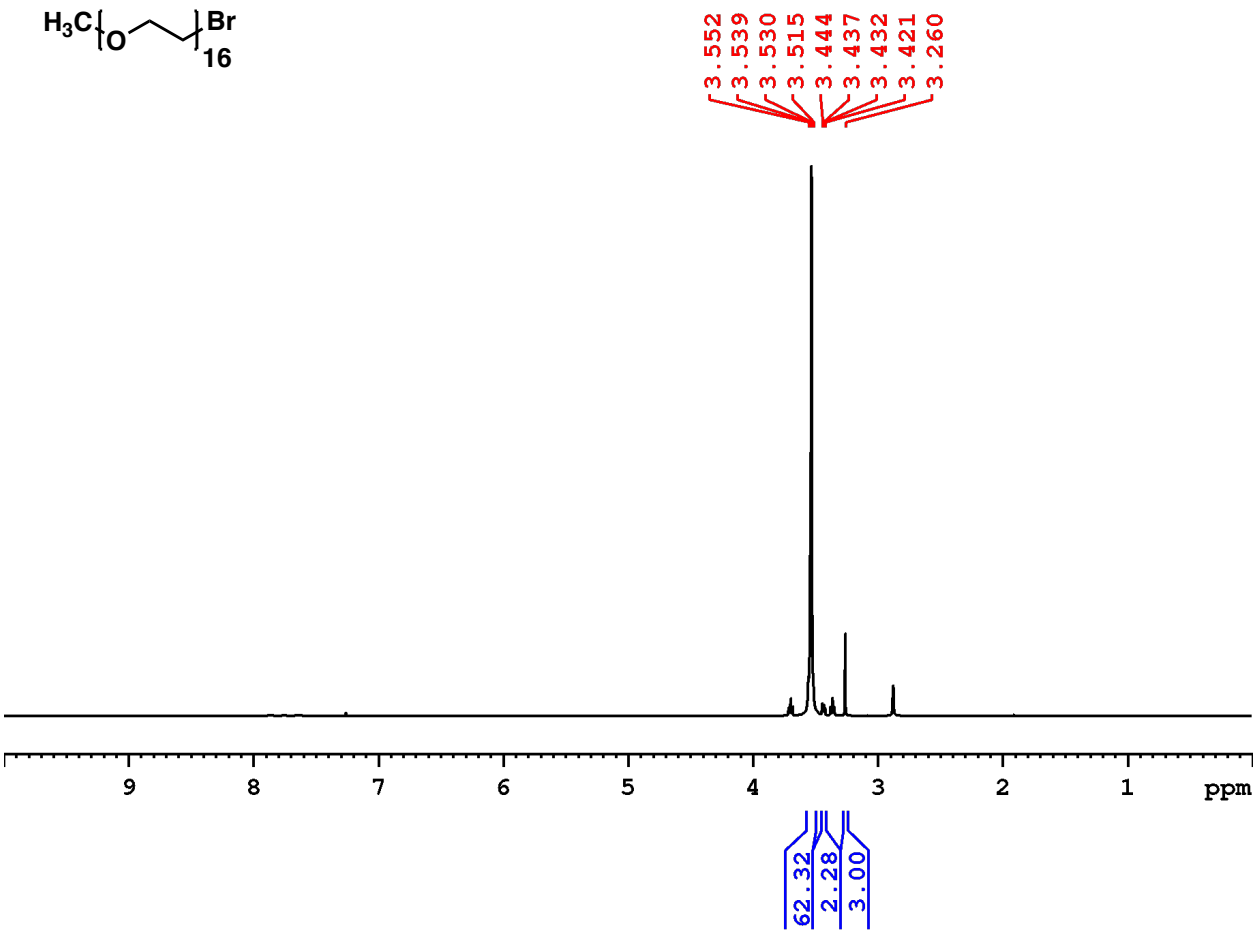

Figure 1-13. ^{1}H NMR spectrum of mPEG-Br in $CDCl_3$.

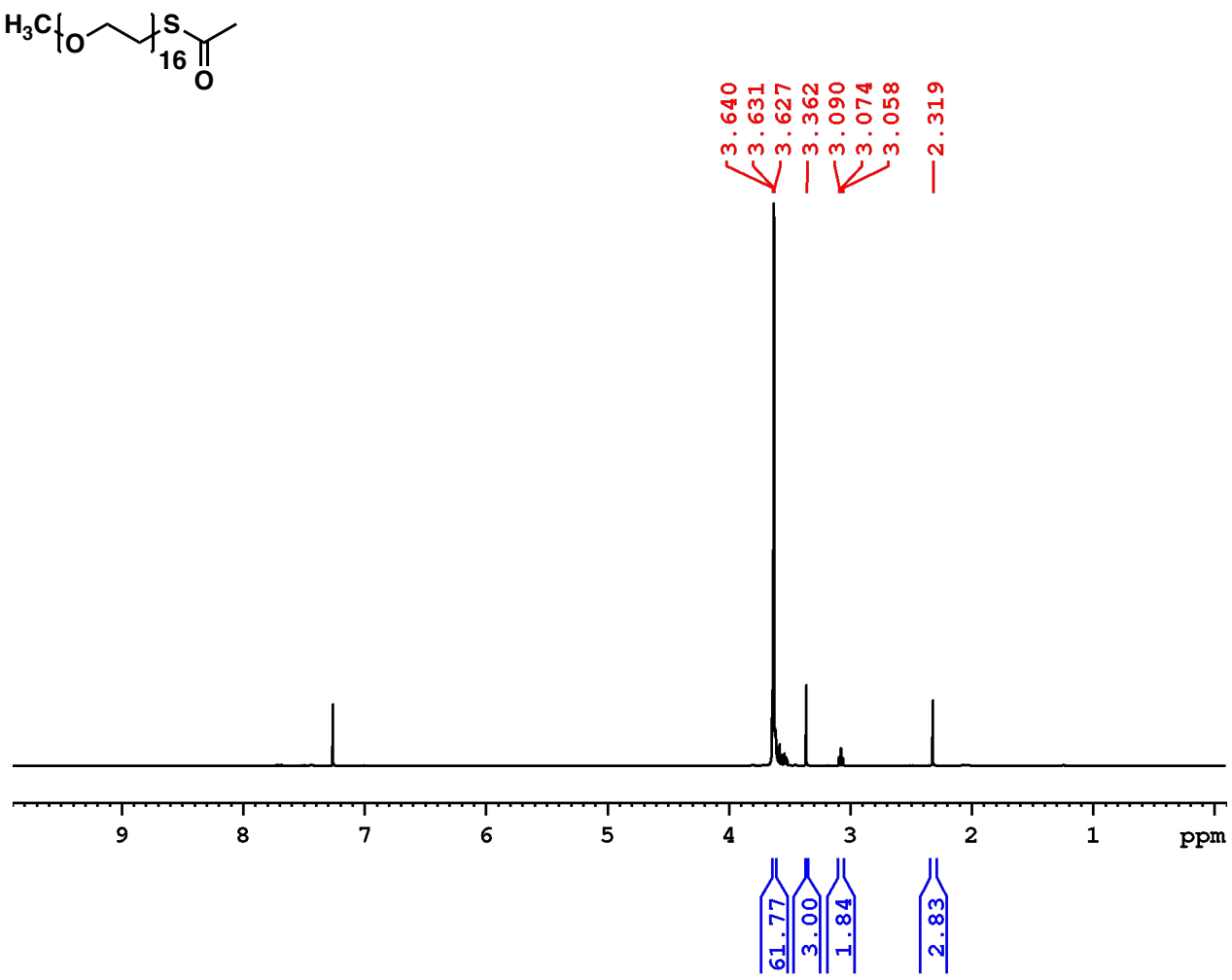

Figure 1-13. ^{1}H NMR spectrum of mPEG-SAc in $CDCl_3$.

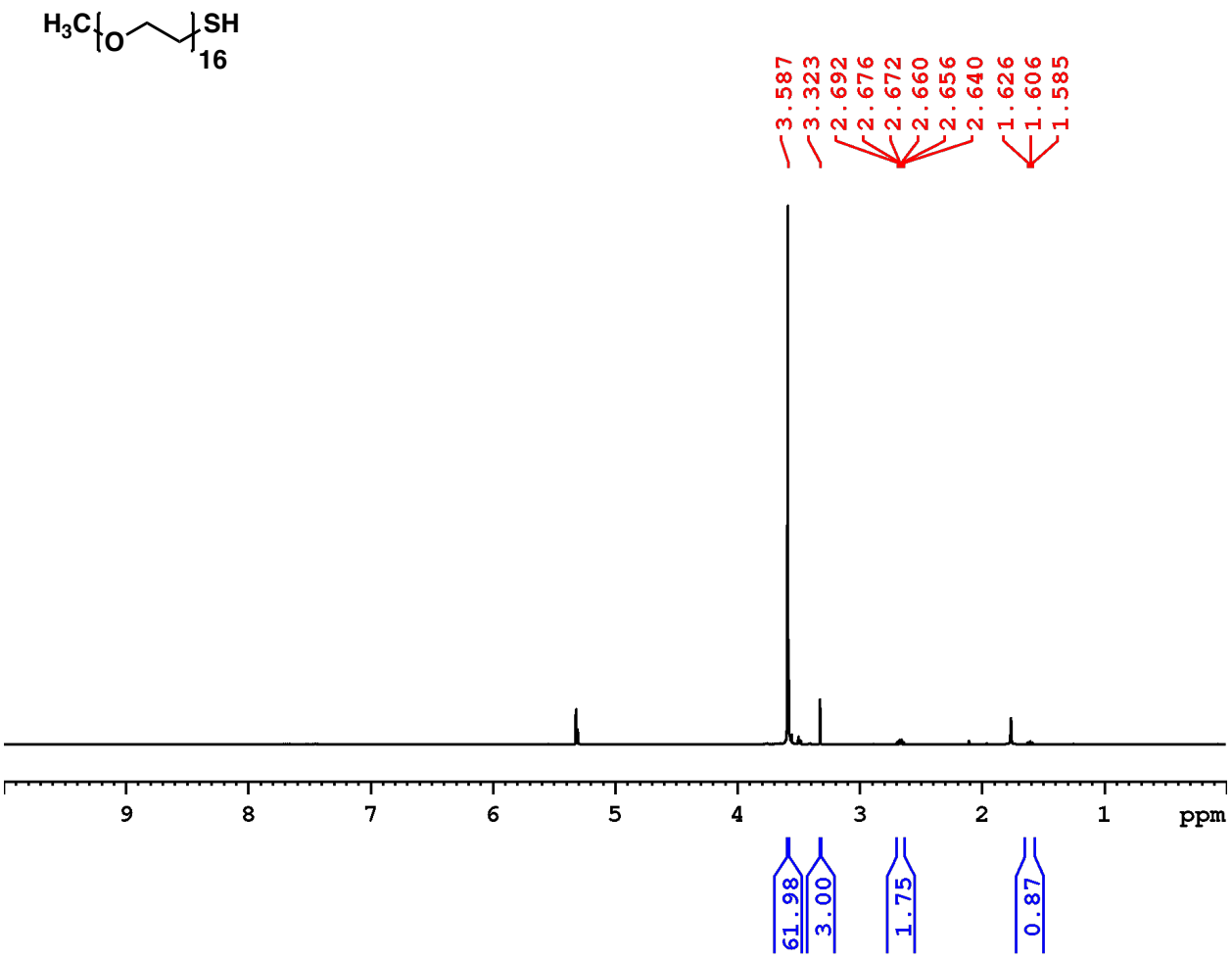

Figure 1-15. ^{1}H NMR spectrum of mPEG-SH in CD_2Cl_2.

1. 4. Discussion and Future Steps

In this work, OCNs were demonstrated to be tunable both in size and surface chemistry. Synthesis of linkers with different sizes enabled modification of the OCN size, whereas synthesis of thiolated ligands such as mPEG-SH facilitated alterations is hydrophilicity of the resulting OCN.

The OCNs made with the G1 linker have altered reactivity towards thiolated ligands, compared to the OCNs made with the G2 linker, potentially due to sterics. To further investigate the role of the linker design in OCN reactivity and also to develop new OCNs, more complicated linkers can be employed. These linkers could have a longer chain of aromatic ring spacers, or have branched structures (**Figure 1-16**). These linkers would facilitate increase in particle size or number of ligand attachment points and result in generation of new OCNs with novel properties.

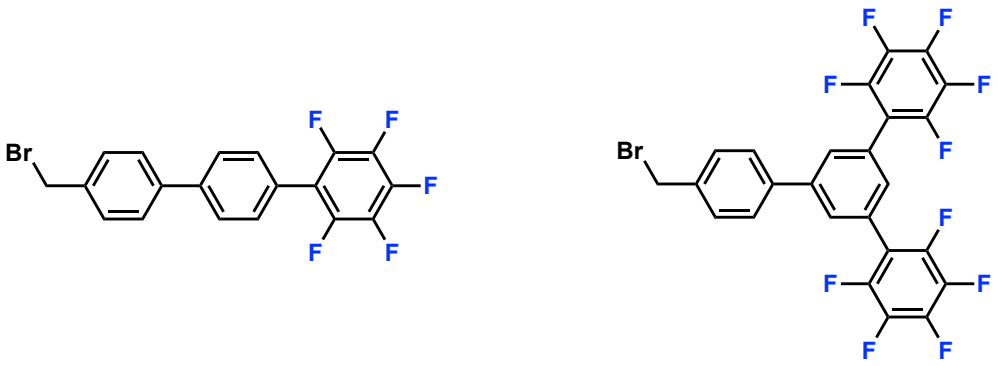

Figure 1-16. The proposed designs of future OCN linkers.

1. 5. References

1. Mammen, M., Choi, S.-K., and Whitesides, G. M. *Angew. Chem. Int. Ed.*, **1998**, 37, 2754-2794.
2. Kiessling, L. L., Gestwicki, J. E., and Strong, L. E. *Angew. Chem. Int. Ed.*, **2006**, 45, 2348-2368.
3. Daniel, M.-C., and Astruc, D. *Chem. Rev.*, **2004**, 104, 293-346.
4. Dreaden, E. C., Alkilany, A. M., Huang, X., Murphy, C. J., and El-Sayed, M. A. *Chem. Soc. Rev.*, **2012**, 41, 2740-2779.
5. Brust, M., Walker, M., Bethell, D., Schiffrin, D. J., and Whyman, R. *J. Chem. Soc*., *Chem. Commun.*, **1994**, 801-802.
6. Love, J. C., Estroff, L. A., Kriebel, J. K., Nuzzo, R. G., and Whitesides, G. M. *Chem. Rev.*, **2005**, 105, 1103-1170.
7. Hostetler, M. J., Green, S. J., Stokes, J. J., and Murray, R. W. *J. Am. Chem. Soc.*, **1996**, 118, 4212-4213.
8. Hostetler, M. J., Templeton, A. C., and Murray, R. W. *Langmuir*, **1999**, 15, 3782–3789.
9. Häkkinen, H. *Nat. Chem.*, **2012**, 4, 443-455.
10. Spokoyny, A. M. *Pure Appl. Chem.*, **2013**, 85, 903-919.
11. Pitochelli, A. R., and Hawthorne, M. F. *J. Am. Chem. Soc.*, **1960**, 82, 3228-3229.
12. Farha, O. K., Julius, R. L., Lee, M. W., Huertas, R. E., Knobler, C. B., and Hawthorne, M. F. *J. Am. Chem. Soc.*, **2005**, 127, 18243-18251.
13. Jalisatgi, S. S., Kulkarni, V. S., Tang, B., Houston, Z. H., Lee Jr., M. W., and Hawthorne, M. F. *J. Am. Chem. Soc.*, **2011**, 133, 12382-12385.

14. Sarma, S. J., Khan, A. A., Goswami, L. N., Jalisatgi, S. S., and Hawthorne, M. F. *Chem. Eur. J.*, **2016**, 22, 12715-12723.

15. Wixtrom, A. I., Shao, Y., Jung, D., Machan, C. W., Kevork, S. N., Qian, E. A., Axtell, J. C., Khan, S. I., Kubiak, C. P., and Spokoyny, A. M. *Inorg. Chem. Front.*, **2016**, 3, 711-717.

16. Birchall, J. M., Green, M., Haszeldine, R. N., and Pitts, A. D. *Chem. Commun. Lond.*, **1967**, 338-339.

17. Becer, C. R., Hoogenboom, R., Schubert, U. S. *Angew. Chem. Int. Ed.*, **2009**, 48, 4900-4908.

18. Becer, C. R., Babiuch, K., Pilz, D., Hornig, S., Heinze, T., Gottschaldt, M., and Schubert, U. S. *Macromolecules*, **2009**, 42, 2387-2394.

19. Spokoyny, A. M., Zou, Y., Ling, J. J., Yu, H., Lin, Y.-S., Pentelute, B. L. *J. Am. Chem. Soc.*, **2013** 135, 5946-5949.

Chapter 2: Towards Development of Histone Deacetylase Inhibitors Featuring Boron Cluster-Based Pharmacophores

2. 1. Introduction

In the nucleus of eukaryotic cells, DNA is wrapped around histone proteins. Each histone complex wraps a short stretch of DNA, approximately 146 base pairs, to form structures known as the nucleosomes. The DNA is packed into the nucleus in repeated units of nucleosomes, which in addition to condensing the DNA, serves as an avenue for regulation of gene transcription.[1] Binding of DNA to histone proteins can potentially interfere with the access of transcription machinery to the DNA and repress gene transcription. This interference is highly dependent on the number of nucleosomes formed in the DNA, as well as the binding affinity between the DNA and the histone protein, and can be modulated by post-translational modification of histones (**Figure 2-1**). The N-terminus of histones are susceptible to post-translational modifications by chromatin remodeling proteins, dictating the binding affinity of histones to the DNA.[2,3]

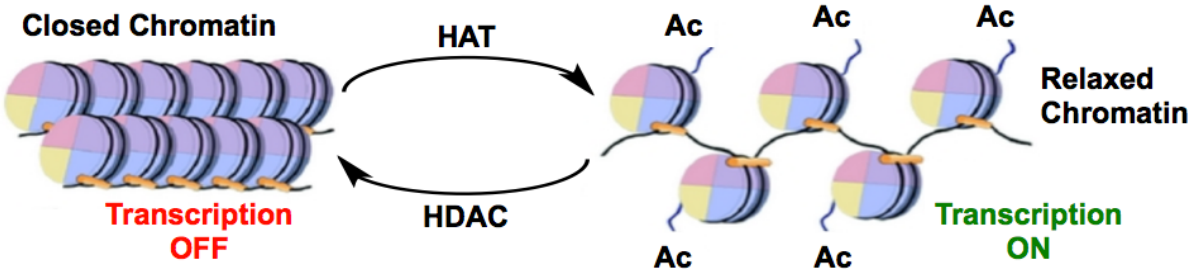

Figure 2-1. Modulation of chromatin structure by chromatin remodeling enzymes. HDACs promote the closed conformation of chromatin and lead to lower transcription level.

Histone deacetylase (HDAC) enzymes are a class of chromatin remodeling proteins that catalyze hydrolysis of acetyl groups off of N-acetylated lysine residues on histone proteins.[4] This transformation leads to a stronger electrostatic interaction between the DNA and histone proteins, condenses nucleosomes, and causes the chromatin to take a closed conformation. Transcription of

the genes in the closed conformation of chromatin is hindered, thus the HDACs operate as regulatory elements for suppression of transcription.[2,3]

Chromatin remodeling enzymes maintain the gene expression homeostasis, determining the genes that can be transcribed and their level of expression in the cell; consequently, defining the function of the cell. As a result, these enzymes are highly regulated. Misregulation is often associated with altered cell function and diseases. Amongst chromatin remodeling enzymes, HDACs are particularly of high importance since abnormal expression of these enzymes has been linked to many neurodegenerative diseases and cancers.[5-8] Furthermore, multiple studies have demonstrated the association between exposure to cocaine and misregulation of HDACs in neurons, particularly in areas of the brain that are involved in reward circuitry and development of addiction.[9,10] As gene regulators, HDACs have the potential to impose extremely stable and long-lasting changes to the function of neurons, a hallmark of cocaine addiction. As a result, HDACs have become a critical target of studies that aim to uncover the underlying cellular mechanism of cocaine addiction.[11]

Despite the established significance of HDACs in cocaine addiction, the link between the two has not been fully characterized yet, primarily due to lack of proper pharmacological tools to study HDACs in the brain.[12] In many of these studies, small-molecule HDAC inhibitors are employed to track and modulate HDACs. However, a majority of HDAC inhibitors suffer from poor blood-brain barrier (BBB) permeability, which hinders *in vivo* monitoring of HDACs.[13] Furthermore, HDACs are a family of enzymes consisting of 19 isoforms.[4] Such diversity expands the pool of HDAC substrates and binding partners, granting the HDACs the power to fine-tune their modulation of chromatin. However, it also complicates investigations into the role of HDACs in cocaine addiction, since each isoform needs to be selectively targeted. The majority of

developed HDAC inhibitors cannot distinguish between different isoforms and as a result are not suitable for cocaine addiction studies.[14,15] Investigation of the association between cocaine addiction and misregulation of HDACs in the brain, calls for development of a new class of HDAC inhibitors that are both isoform-selective and BBB permeable.

Research into development of small-molecule HDAC inhibitors has led to the discovery of effective inhibitors of HDACs. The design of many of these inhibitors follows the cap-linker-chelator model (**Figure 2-2a**). In this model, the inhibitor is composed of three parts. First, a zinc-chelating group that docks inside the HDAC active site and binds to the zinc atom located there. Second, a cap group that interacts with hydrophobic surface residues on the surface of HDAC protein and facilitates recognition and selectivity. Third, a linker moiety attaching the cap group to the chelator end (**Figure 2-2b**).[16] The cap-linker-chelator model has led to discovery of potent inhibitors such as Vorinostat and Panobinostat, both FDA approved cancer treatment agents.[17,18] Nevertheless, neither one of these inhibitors are able to effectively breach the BBB.

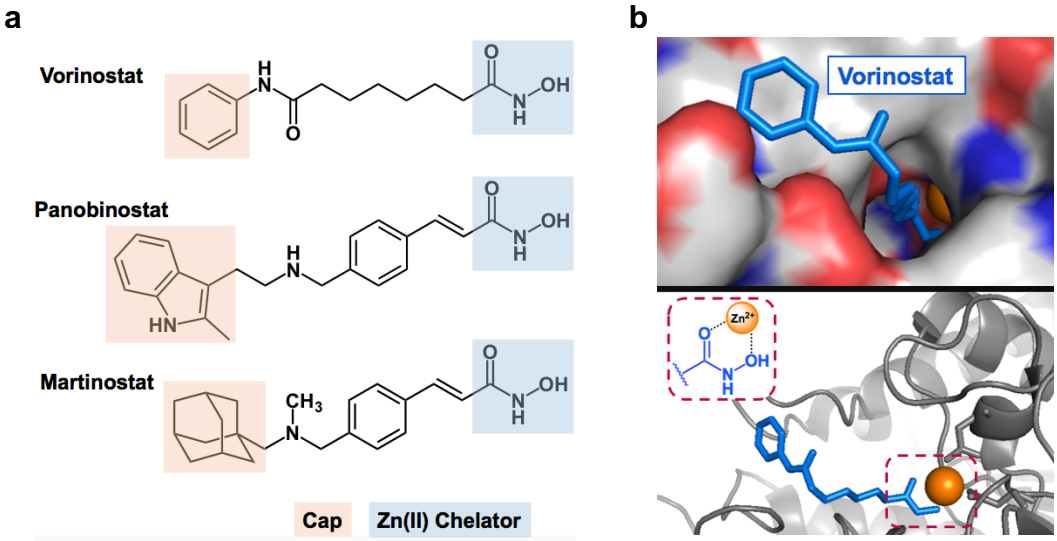

Figure 2-2. Panel **a** presents the structure of three potent HDAC inhibitors. The design of all three follows the cap-linker-chelator model. Panel **b** demonstrates the crystal structure of HDAC2 in complex with Vorinostat (PDB ID 4LXZ). The chelator sits inside the tunnel-shaped active site while the cap group interacts with surface residues.

In fact, to date, only a single example of a BBB permeable HDAC inhibitor has been reported. This inhibitor, known as Martinostat, was developed in 2014 by Hooker and coworkers and was successfully employed to non-invasively image HDACs in the central nervous system (CNS).[19-21] The structure of Martinostat follows the well-known cap-linker-chelator model and displays three key features: 1) a hydroxamic acid moiety as the chelator to target the active site of HDAC, 2) an adamantyl hydrophobic cap group to potentially increase the cell, nuclear, and BBB permeability, and 3) a radioactive ^{11}C label for *in vivo* tracing by positron emission tomography (PET) (**Figure 2-3**). It has been postulated that the incorporation of the highly hydrophobic three-dimensional adamantane group has been the most contributing factor to the BBB permeability of Martinostat.[19]

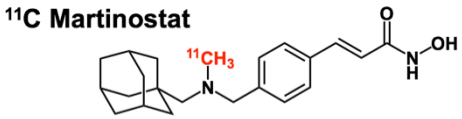

Figure 2-3. Martinostat labeled with ^{11}C for *in vivo* PET imaging.

Although Martinostat has been a tremendous advancement for *in vivo* imaging of HDACs in the CNS, this inhibitor lacks the isoform-selectivity needed for implementation in cocaine addiction studies. In vitro binding assays with nine HDAC isoforms have determined that Martinostat has similar affinity for HDAC isoforms 1, 2, 3, and 6.[19] Thus, the structure of Martinostat needs modifications in such manner that retains its BBB permeability, but alters the interactions between molecule and protein surface to establish isoform-selectivity. Since the cap group is involved in surface interaction, the best method to achieve isoform-selectivity is to selectively adjust the electronics of the cap group through chemical functionalization. Despite exhibiting the desired lipophilicity needed for membrane transport, Martinostat's adamantane group is not well suited for functionalization. The C-H vertices lend few synthetic strategies to modification. However, icosahedral carboranes ($C_2B_{10}H_{12}$), which are isosteric to adamantyl

groups, are amenable to functionalization and may serve as an appropriate substitute for the adamantyl group for development of isoform-selective BBB permeable HDAC inhibitors.[22]

Carboranes are a class of robust cluster molecules with interesting features such as three-dimensional aromaticity and exceptional stability. Carborane is often regarded as the 3D analogue of benzene, and offers a large surface area for hydrophobic interactions. Furthermore, the polarity of carborane is highly tunable through chemical functionalization, due to electron delocalization on the surface of carborane cluster (**Figure 2-4**).[23-25] Such characteristics are highly desirable in drug development; thus, incorporation of carboranes in design of pharmaceuticals, specifically as adamantane substitutes, has been an active area of research since it was first proposed by Plešek in 1992.[25,26]

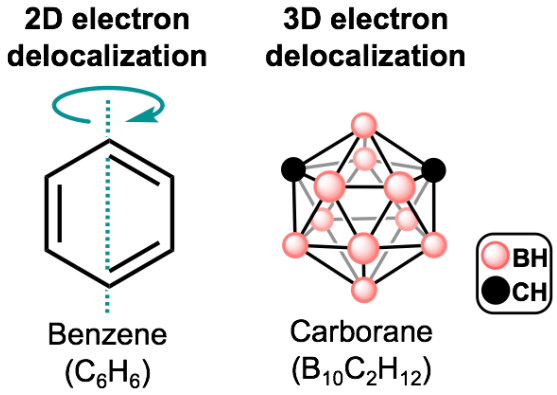

Figure 2-4. Carboranes are 3D aromatic analogues of benzene. These boron-rich clusters are extremely stable as a result of electron delocalization on their surface. The carborane shown in this figure is specifically a *meta* isomer as determined by the placement of its carbon vertices.

Unfortunately, limited scope of chemical modifications on carboranes has been a major setback to the establishment of carboranes as widely utilized pharmacophores. Recently, new chemical methods have emerged for efficient vertex-differentiated and dense functionalization of carborane clusters, facilitating potential use of carboranes as highly tunable 3-dimentional

scaffolds.[27,28] As a result, we aim to synthesize a Martinostat analogue, Carboranostat I, in order to determine if we can develop an HDAC inhibitor with the potential of BBB permeability and isoform-specificity (**Figure 2-5**). Herein, we report synthesis and characterization of Carboranostat I, as well as its inhibitory activity towards HDAC enzyme.

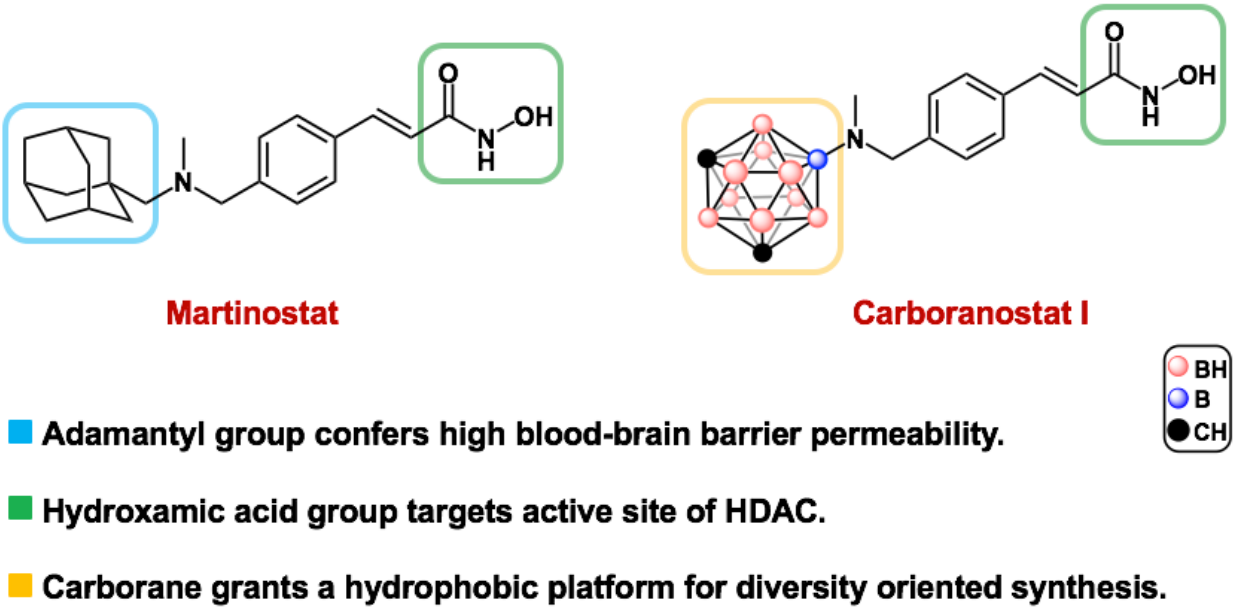

Figure 2-5. The structure of the proposed HDAC inhibitor, Carboranostat I, resembles Martinostat. The carborane, however, can be densely functionalized, providing a substantial chemical space for diversity oriented synthesis and leading to potential development of BBB permeable, isoform-specific HDAC inhibitors.

2. 2. Methods

2. 2. 1. Synthesis of Martinostat

General Considerations

The synthetic scheme for synthesis of Martinostat is depicted in **Figure 2-6**. This synthetic scheme is adapted from reports by Wang *et al.*.[19] Compound 1 was synthesized based on the report by Zhdanko *et al.*.[29] The 1-adamantane carbonitrile used in synthesis of 1P was purchased from Alfa Aesar.

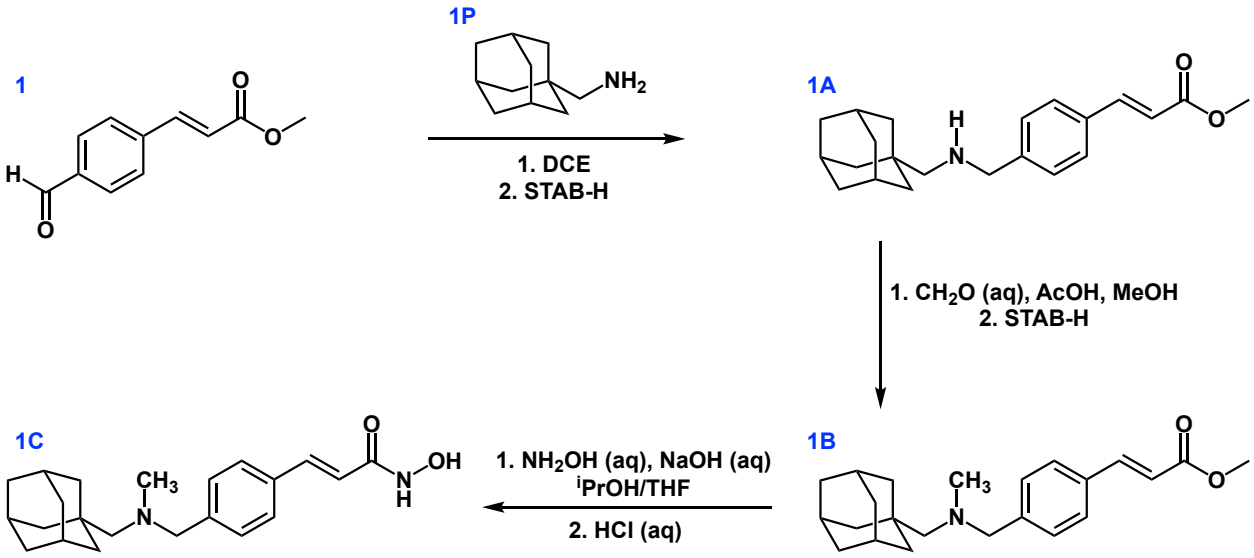

Figure 2-6. General scheme for synthesis of Martinostat (compound 1C).

Synthesis of 1P

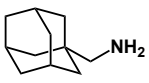

To a solution of $LiAlH_4$ (1.88 g, 49.6 mmol) in 80 mL dry diethyl ether, 1-adamantane carbonitrile (2.00 g, 12.4 mmol) dissolved in 30mL dry diethyl ether was added at 0°C. After 30 minutes the reaction was warmed up to room temperature and left to stir overnight under a positive flow of

nitrogen. The reaction mixture was then exposed to air, cooled to 0°C, and 1.88 mL H_2O, 1.88 mL 15% NaOH, and 5.64 mL H_2O were added stepwise and very carefully to the reaction mixture. Stirring is continued until a white precipitate is formed. The mixture was then filtered through a glass frit and washed with 30mL diethyl ether. The filtrate was dried in air providing 1P as a white solid (1.89 g, 92%).

Synthesis of 1A

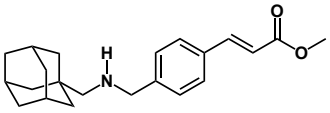

To a mixture of 1P (1.50 g, 9.08 mmol) and 1 (1.57 g, 8.25 mmol) in a round bottom flask, 50 mL dichloroethane was added and the solution was stirred overnight at room temperature. Upon confirmation of imine formation via ^{1}H NMR, the solution was cooled to 0°C and sodium triacetoxyborohydride (3.85 g, 18.15 mmol) was added. After 45 minutes, the solution was warmed up to room temperature and stirred overnight. The reaction was quenched by addition of 100 mL of 0.5M $NaHCO_3$. The organic layer was separated and treated with another 100 mL of 0.5M $NaHCO_3$. Next, the organic layer was washed with 50 mL of DI water and dried over $MgSO_4$. The mixture was filtered through Celite on a glass frit and dried *in vacuo* providing a yellow oil. The oil was dissolved in 5mL methanol and cooled to -15°C for at least 15 minutes. The white precipitate was filtered off and washed with cold methanol and cold diethyl ether to obtain the product 1A (2.12 g, 76%).

Synthesis of 1B

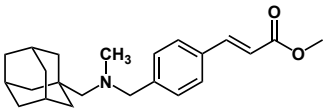

To a solution of 1A (1.500 g, 4.42 mmol) in 90 mL methanol, formaldehyde (37% aqueous, 6 mL) was added followed by 0.30 mL acetic acid. The solution was stirred at room temperature for 2 hours. The reaction mixture was cooled to 0°C and sodium triacetoxyborohydride (4.686 g, 22.11 mmol) was added. After 45 minutes, the solution was warmed up to room temperature and stirred overnight. The solvent was then removed and the residue was dissolved in 100 mL methylene chloride and washed twice with 30 mL portions of saturated $NaHCO_3$. The organic layer was washed with 50 mL DI water and then dried over $MgSO_4$. The mixture was filtered through Celite on a glass frit and dried *in vacuo* providing a yellow oil. The oil was dissolved in minimal amount of 2:1 MeOH:Et_2O solution and cooled at -15°C. The product, 1B, precipitated out of solution in form of white crystals (1.2773 g, 82%).

Synthesis of 1C (Martinostat)

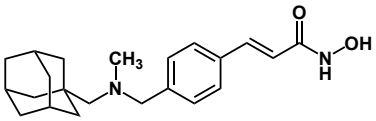

1B (338 mg, 0.956 mmol, 1eq) was dissolved in 4 mL of 1:1 ^{i}PrOH:THF mixture. The solution was cooled to 0°C. Hydroxylamine (50% aqueous solution, 2.05 mL, 33.46 mmol, 35eq) and 1M NaOH (1.34 mL, 1.4eq) were added to the mixture, yielding a clear yellow solution. The solution was stirred at 0°C for 2.5 hours and then at room temperature for 4 hours. Next, the organic solvents were removed *in vacuo*, leaving a cloudy aqueous solution with pH around 12-13 (as

measured by pH paper). Upon treatment with 1M HCl a white solid precipitate forms. Addition of HCl was continued until the solution turned neutral (pH 7 as indicated by pH paper). The supernatant was removed and the solid was washed with small portions of water 5 times. The solid was then lyophilized producing 1C as white powder (323 mg, 95%).

2. 2. 2. Synthesis of Carboranostat I

Carboranostat I was synthesized through the reaction scheme depicted in **Figure 2-7**. Compound 1 was synthesized based on the report by Zhdanko *et al.*.[29] Compound 3P was prepared based on the report by Dziedic *et al.*.[27]

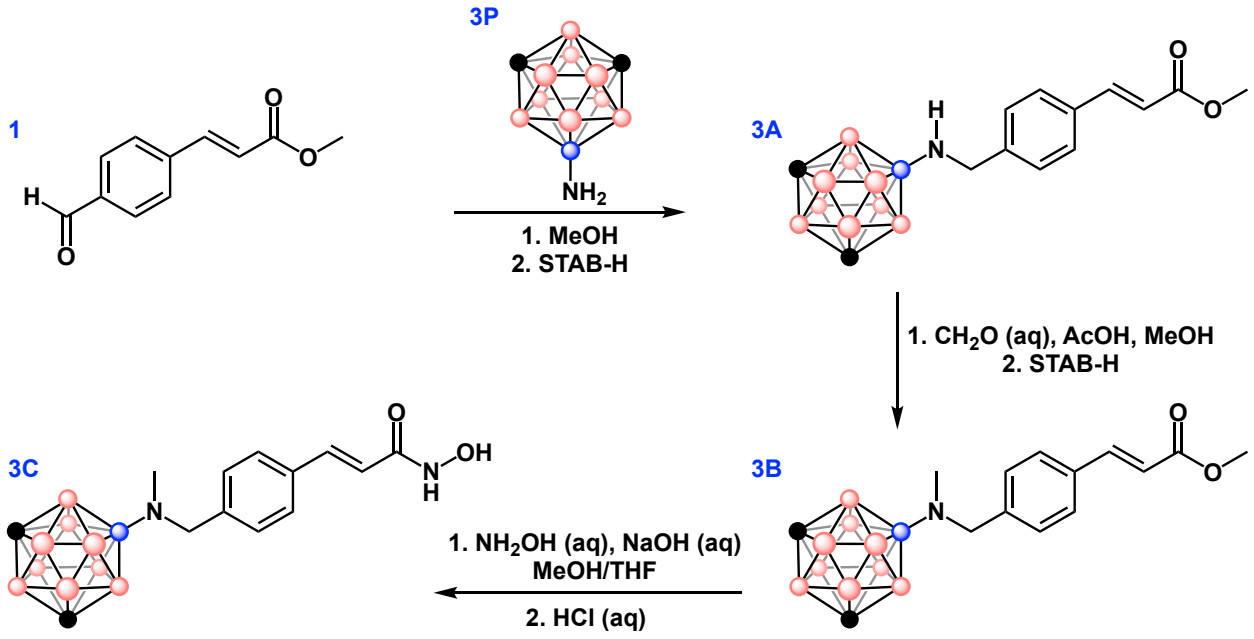

Figure 2-7. General scheme for synthesis of Carboranostat I (compound 3C).

Synthesis of 3A

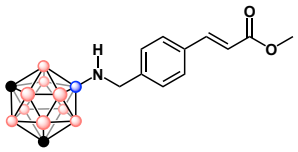

3P (300 mg, 1.88 mmol, 1.1eq) and 1 (326 mg, 1.71 mmol, 1eq) were added to an oven-dried schlenk flask with a stir bar. The flask was purged with nitrogen 5 times. 30 mL dry methanol was syringed into the flask. The reaction was stirred for 2 days at room temperature until ^{1}H NMR spectroscopy revealed complete conversion of 1 to the imine intermediate. Then the reaction mixture was cooled to 0°C and sodium triacetoxyborohydride (542 mg, 2.56 mmol, 1.5eq) was added to the solution under a positive flow of nitrogen. After 45 minutes, the solution was warmed up to room temperature and stirred overnight. The solvent was removed and the yellow residue was dissolved in 20 mL diethyl ether and washed with 20 mL DI water. The aqueous layer was extracted with 20 mL methylene chloride. The organic layers were combined and washed again 20 mL of DI water. The organic layer was dried over $MgSO_4$. The mixture was filtered through Celite on a glass frit and dried *in vacuo* providing the product 3A as a mixture (464 mg, 81%).

Synthesis of 3B

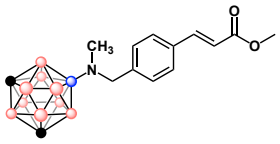

To a solution of 3A (460 mg, 1.38 mmol) in 25 mL methanol, formaldehyde (37% aqueous, 1.85 mL) was added followed by 92 µL acetic acid. The solution was stirred at room temperature for 2 hours. The reaction mixture was cooled to 0°C and sodium triacetoxyborohydride (440 mg, 2.08

mmol) was added. After 45 minutes, the solution was warmed up to room temperature and stirred overnight. The solvent was then removed and the residue was dissolved in 25 mL methylene chloride and washed three times with 25 mL portions of DI water. The organic layer was dried over $MgSO_4$ and the mixture was filtered through Celite on a glass frit and dried *in vacuo* providing a yellow oil. The oil was purified via flash chromatography (eluent: 20% EtOAc in hexanes; R_f = 0.6) through a silica column, using $PdCl_2$ in HCl stain for visualization. The fractions containing the desired product were combined and dried. The residue was dissolved in minimal amount of 3:1 MeOH:Et_2O solution. The product, 3B, precipitated out of solution in form of white crystals (111 mg, 23%).

Synthesis of 3C (Carboranostat I)

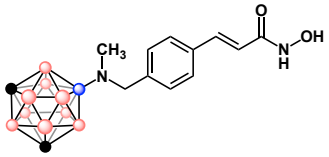

3B (100 mg, 0.288 mmol, 1eq) was dissolved in 1.22 mL of 1:1 MeOH:THF mixture. The solution was cooled to 0°C. Hydroxylamine (50% aqueous solution, 610 µL, 10.073 mmol, 35eq) and 1M NaOH (407 µL, 1.43eq) were added to the mixture, yielding a clear light yellow solution. The solution was stirred at 0°C for 2 hours and then at room temperature for 2 hours. Next, the organic solvents were removed *in vacuo*, leaving a cloudy aqueous solution. Upon treatment with 1M HCl a white solid precipitate forms. Addition of HCl was continued until the solution turned neutral (pH 7 as indicated by pH paper). The supernatant was removed and the solid was washed with small portions of water 5 times. The solid was then lyophilized producing 3C as white powder (81 mg, 81%).

2. 2. 3. HDAC Binding Assay

In order to assess the activity of the synthesized compounds towards inhibition of HDAC proteins *in vitro*, a fluorogenic HDAC assay kit was used. The kit was purchased from BPS Biosciences (cat# 50033) and used as instructed by the directions. The inhibitory activity of Martinostat and Carboranostat I towards HDAC2 enzyme was measured.

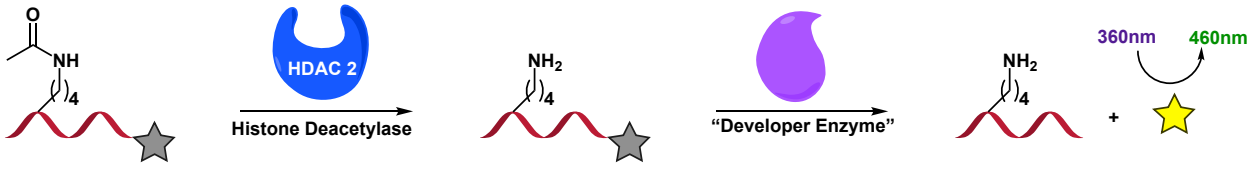

Figure 2-8. Fluorogenic HDAC assay kit can measure the potency of a test inhibitor through generation a fluorescence signal.

In short, the kit functions through an indirect measurement of HDAC activity (**Figure 2-8**). First, the desired inhibitor is incubated with HDAC2 and a peptide substrate. The peptide substrate is a short peptide with an acetylated lysine incorporated in the sequence. The peptide substrate is also covalently attached to a fluorophore. The fluorophore is quenched a result of the covalent linkage to the peptide. HDAC2 can deacetylase the substrate, however, based on the potency and concentration of the inhibitor incubated with the enzyme, the deacetylation of substrate will be hindered. The deacetylation reaction continues for 30 minutes, after which the HDAC activity is fully abolished by addition of a known and potent HDAC2 inhibitor (Trichostatin A) at high concentrations. Then the "developer enzyme" solution is added. The "developer enzyme" selectively breaks the covalent linkage between the fluorophore and the deacetylated peptide. Specifically, the developer will not break the linkage between the fluorophore and an acetylated peptide (intact substrate). Thus, the concentration of the fluorophore released is directly

proportional to HDAC activity during the deacetylation reaction. The higher fluorescence detected determines a higher HDAC activity, and as a result a lower inhibitor potency. Assessment of the fluorescence at various concentrations of a test inhibitor provides a measure for potency of the inhibitor.

2. 3. Results

2. 3. 1. Characterization of Martinostat

Compound 1P was characterized by ^{1}H (**Figure 2-9**) and $^{13}C\{H\}$ (**Figure 2-10**) NMR spectroscopy. 1A was also characterized by ^{1}H (**Figure 2-11**) and $^{13}C\{H\}$ (**Figure 2-12**) NMR spectroscopy. Compound 1B was characterized by ^{1}H (**Figure 2-13**) and $^{13}C\{H\}$ (**Figure 2-14**) NMR spectroscopy, as well as LCMS (**Figure 2-15**). Similarly, 1C was characterized by ^{1}H (**Figure 2-16**) and $^{13}C\{H\}$ (**Figure 2-17**) NMR spectroscopy, and LCMS (**Figure 2-18**).

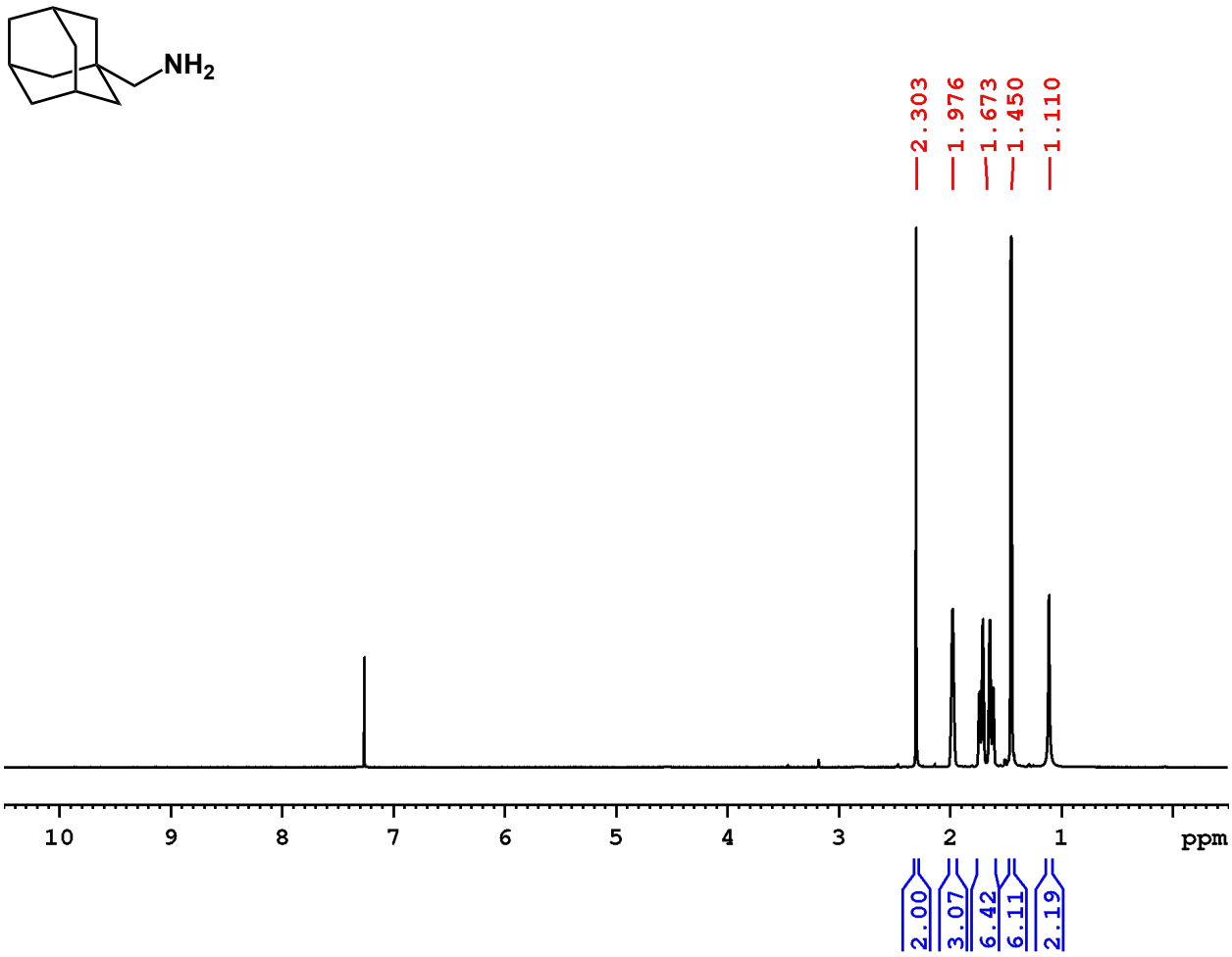

Figure 2-9. ^{1}H NMR spectrum of compound 1P in $CDCl_3$.

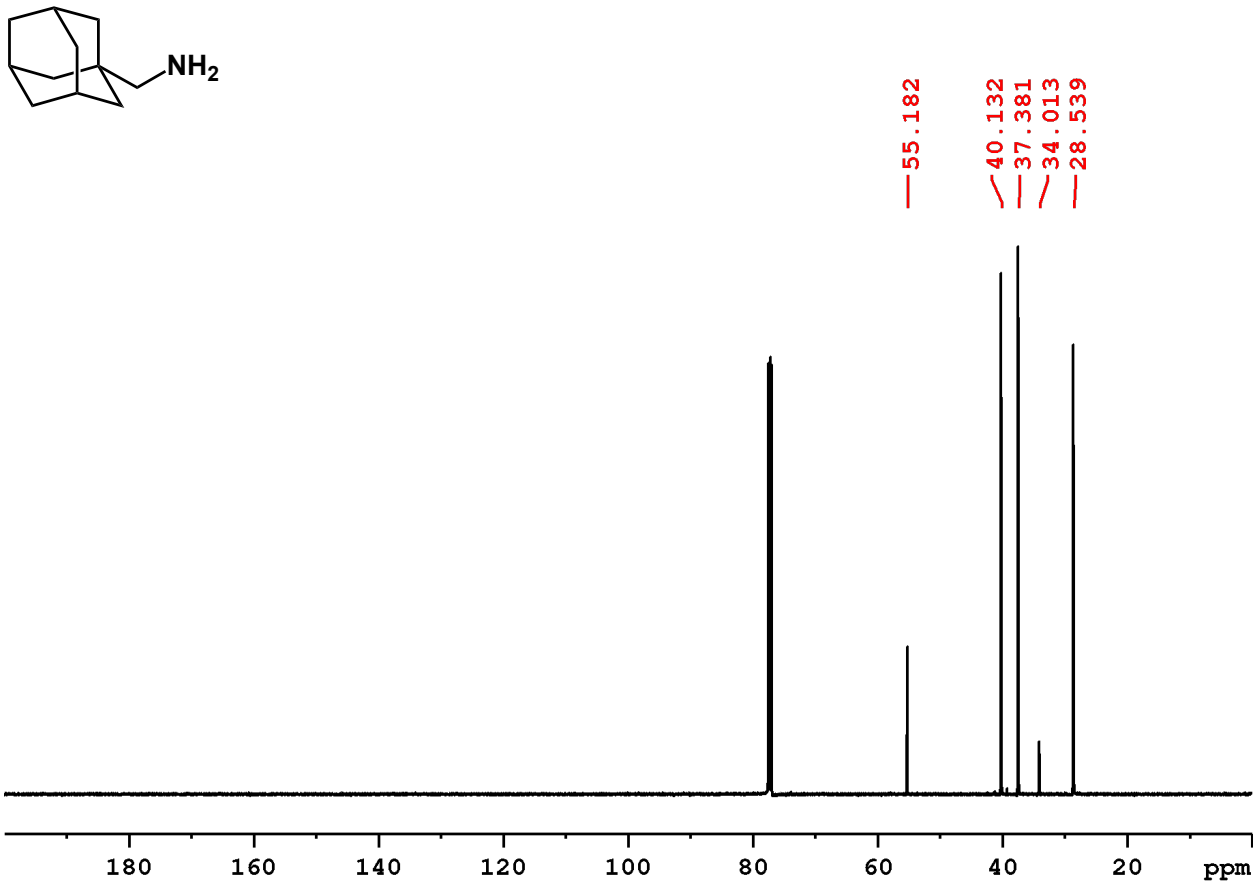

Figure 2-10. $^{13}C\{^{1}H\}$ NMR spectrum of compound 1P in $CDCl_3$.

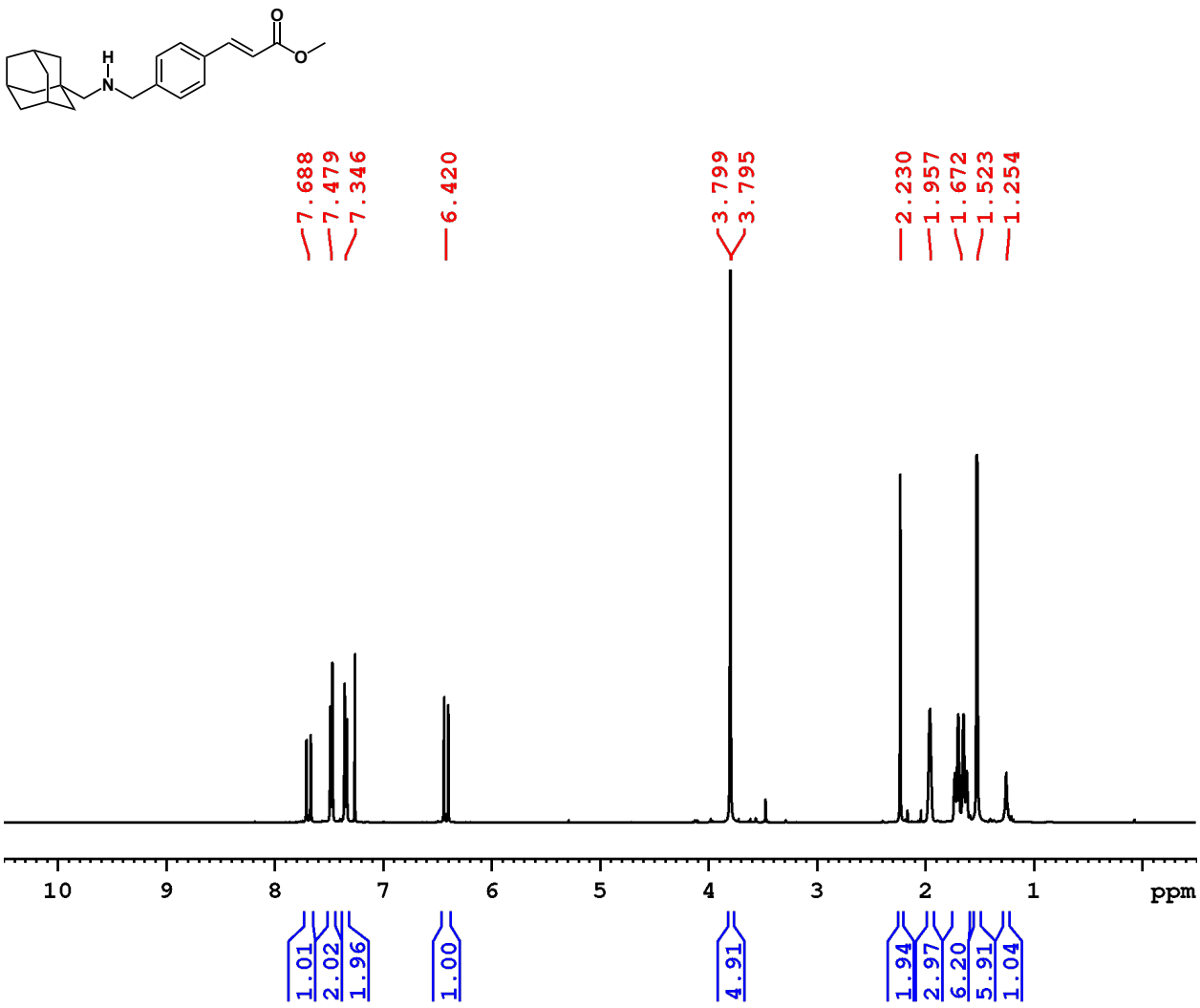

Figure 2-11. ^{1}H NMR spectrum of compound 1A in $CDCl_3$.

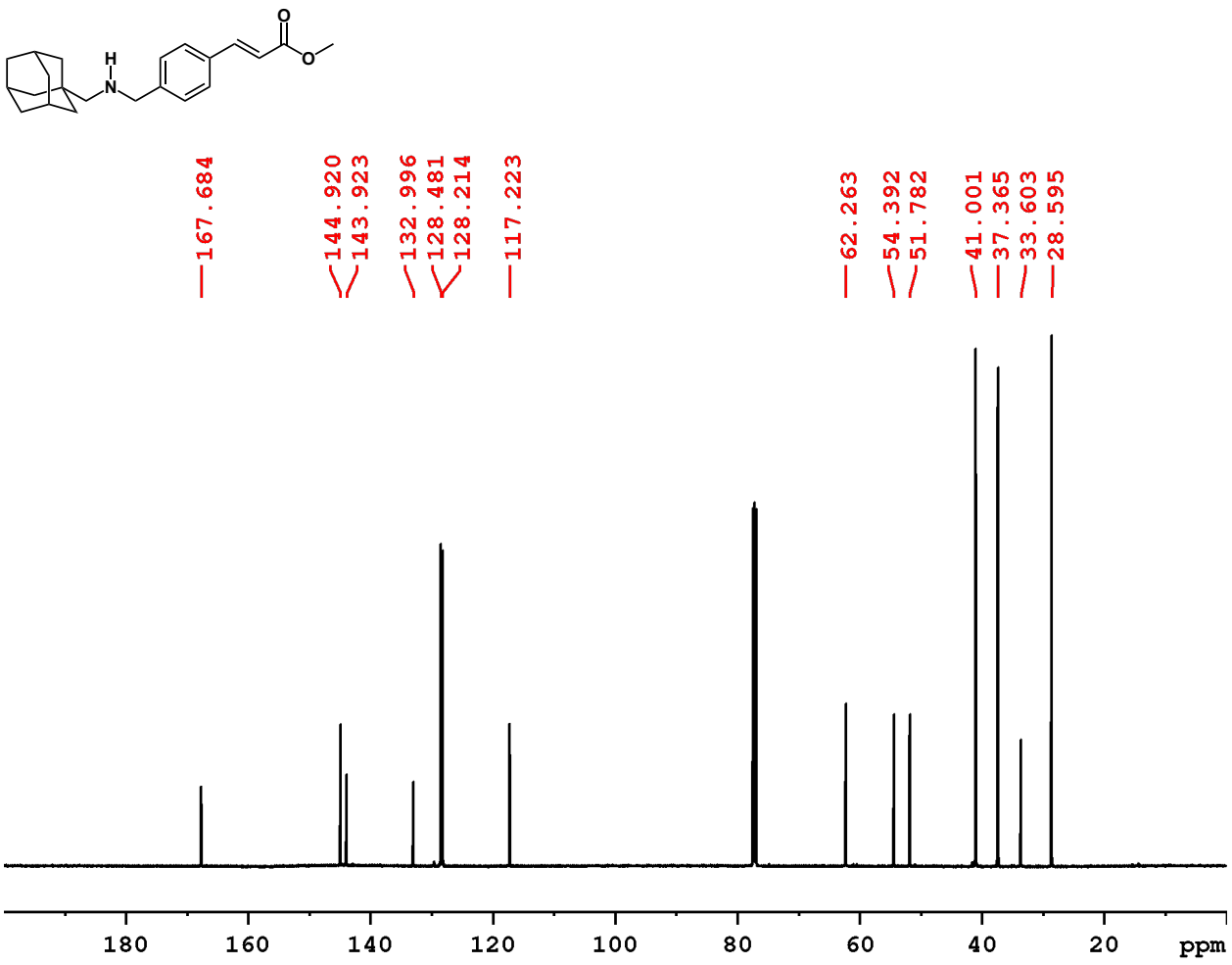

Figure 2-12. $^{13}C\{^{1}H\}$ NMR spectrum of compound 1A in $CDCl_3$.

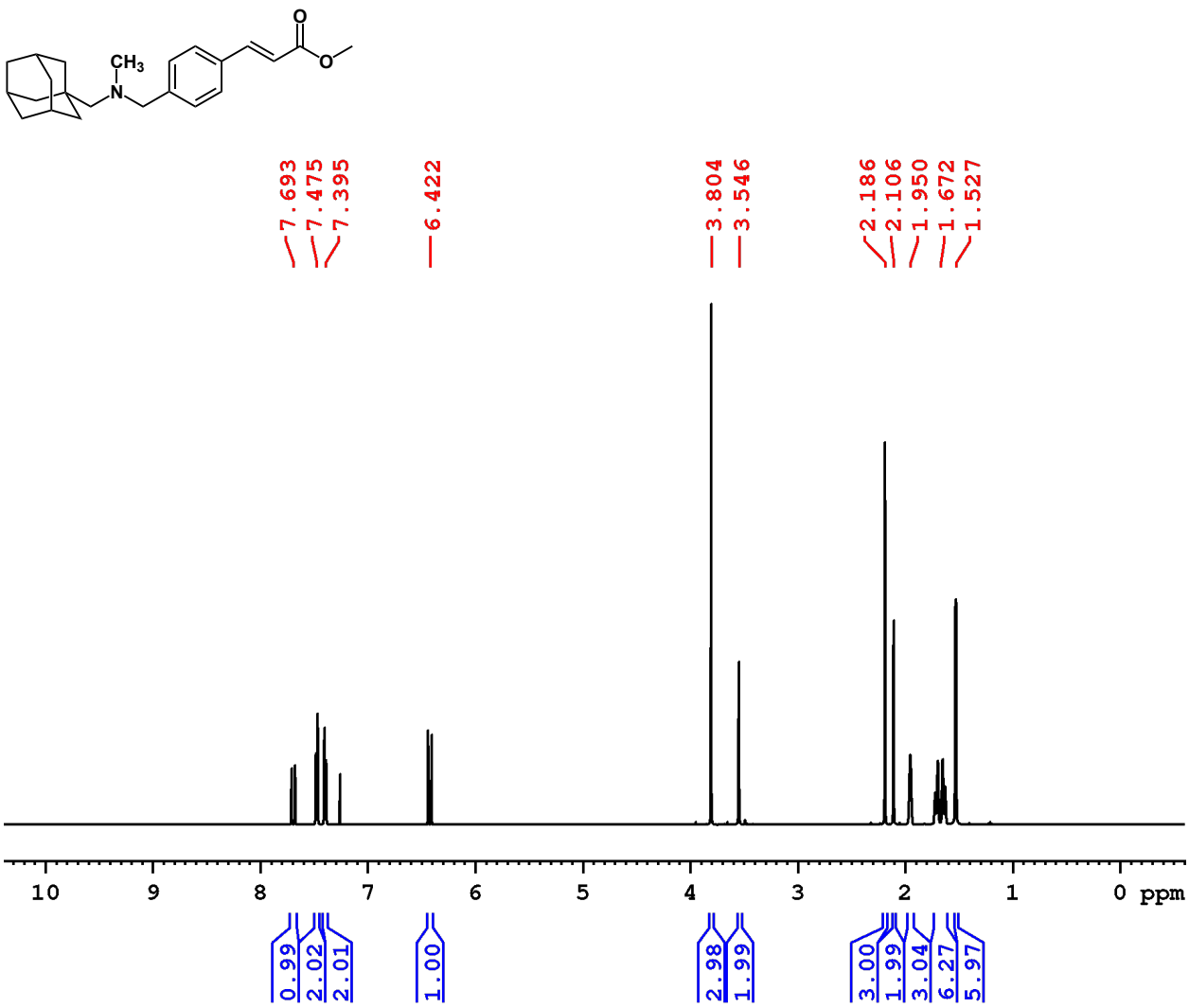

Figure 2-13. ^{1}H NMR spectrum of compound 1B in $CDCl_3$.

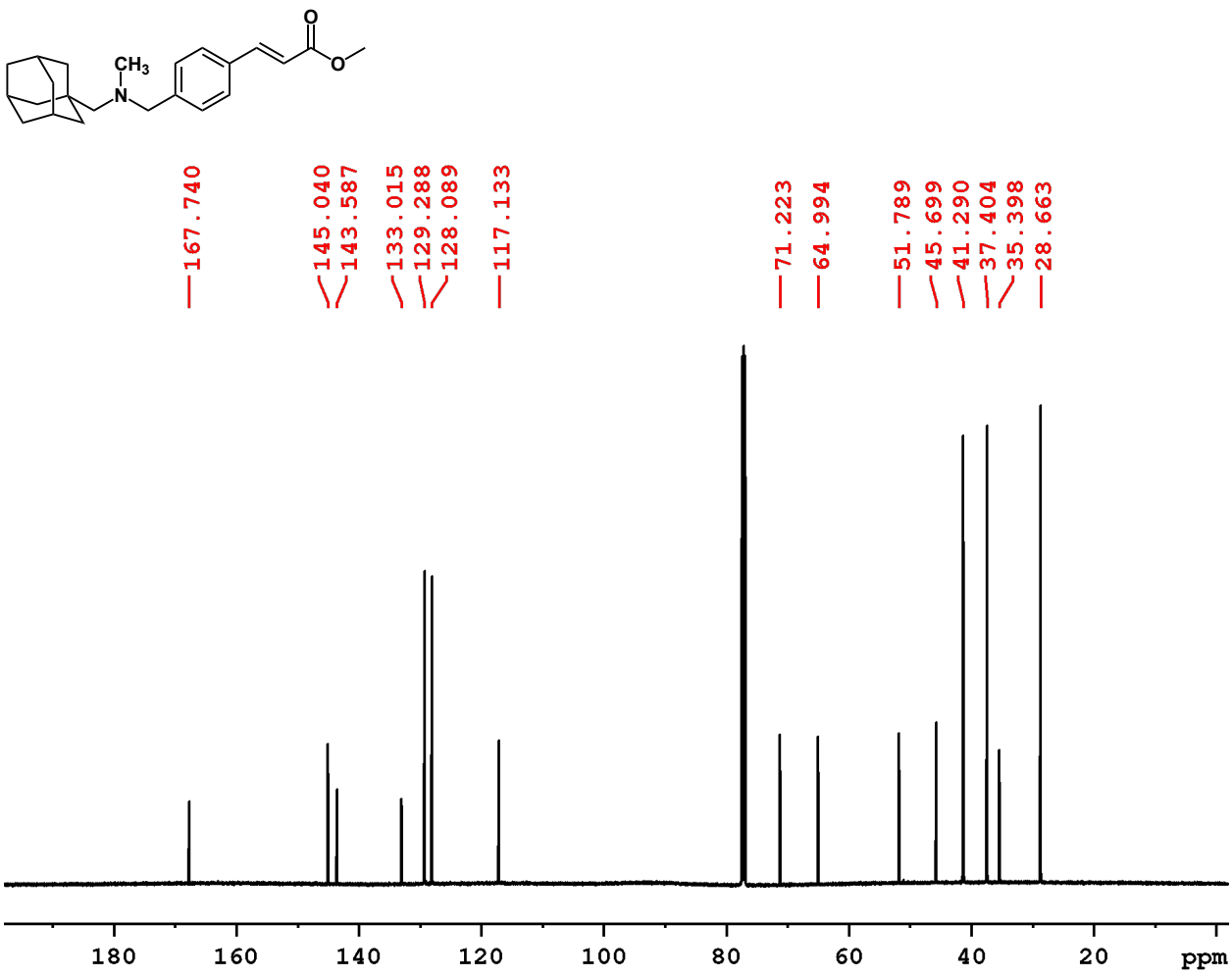

Figure 2-14. $^{13}C\{^{1}H\}$ NMR spectrum of compound 1B in $CDCl_3$.

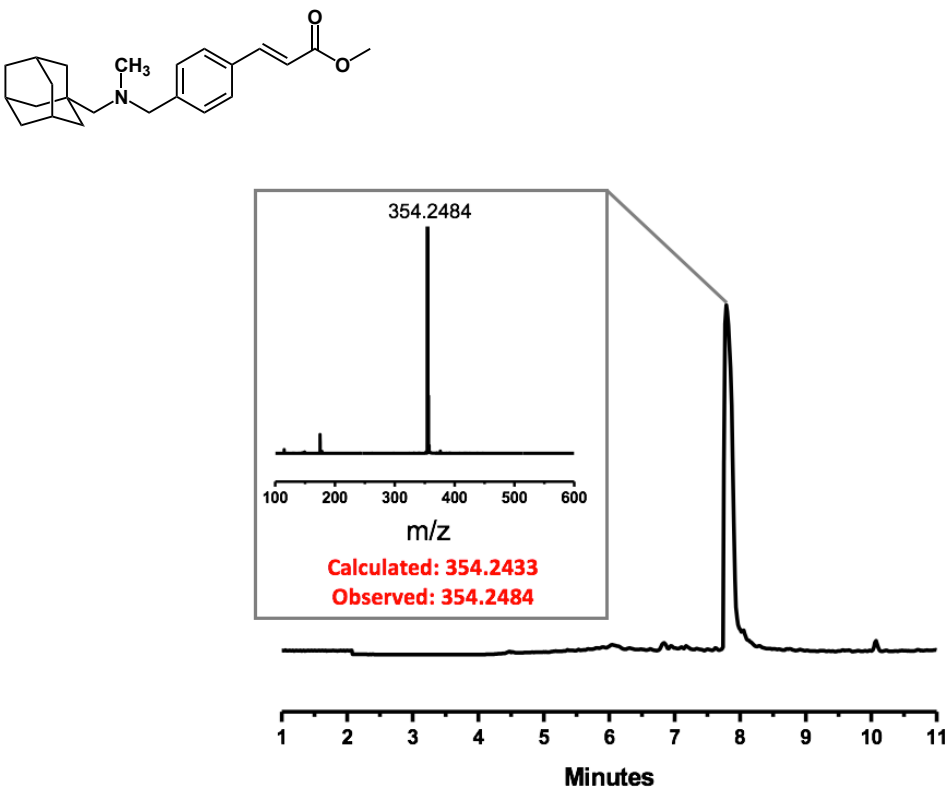

Figure 2-15. LCMS TIC trace for 1B including mass spectrum.

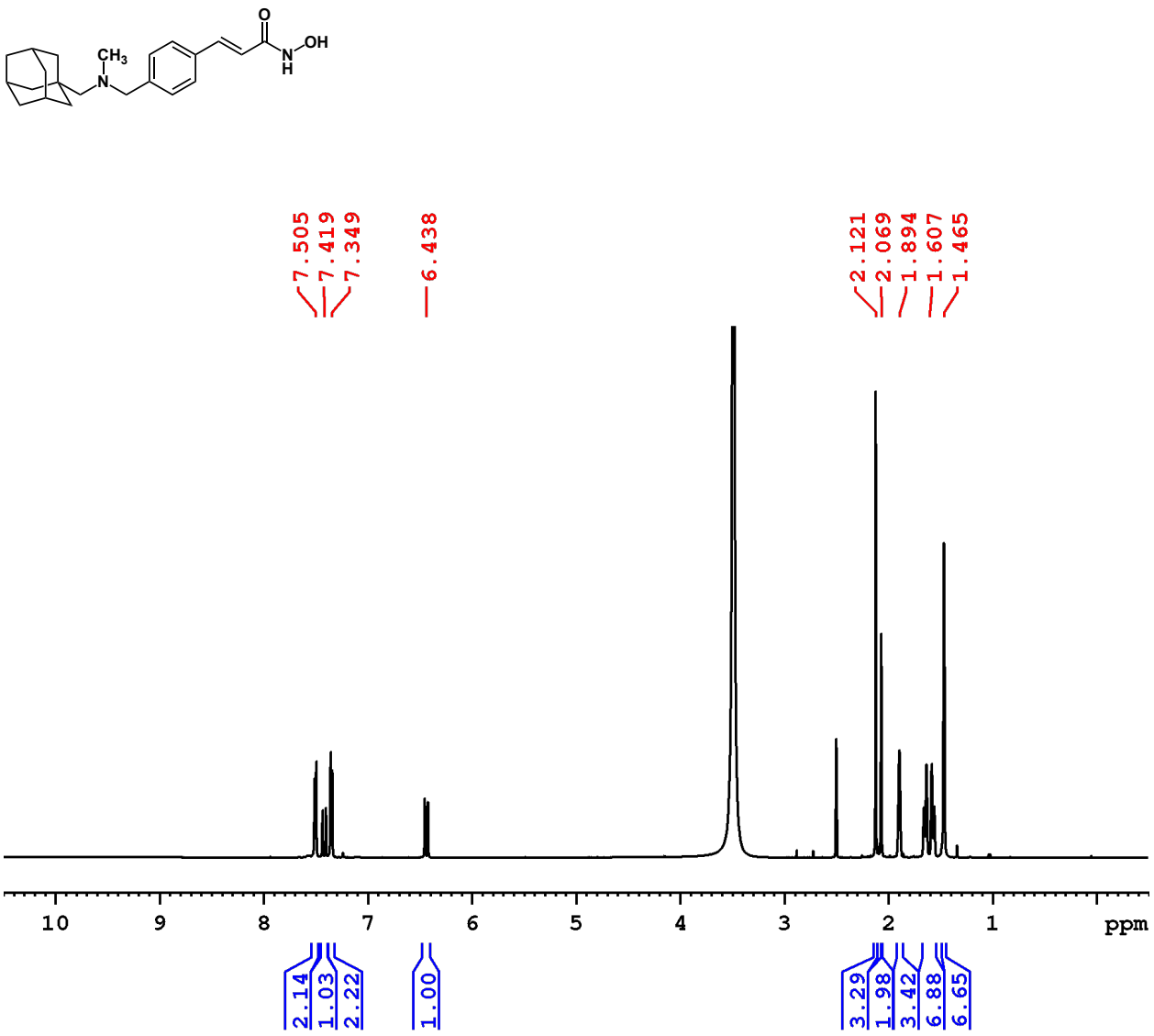

Figure 2-16. ^{1}H NMR spectrum of compound 1C in DMSO-d. Peak at 3.49 is water.

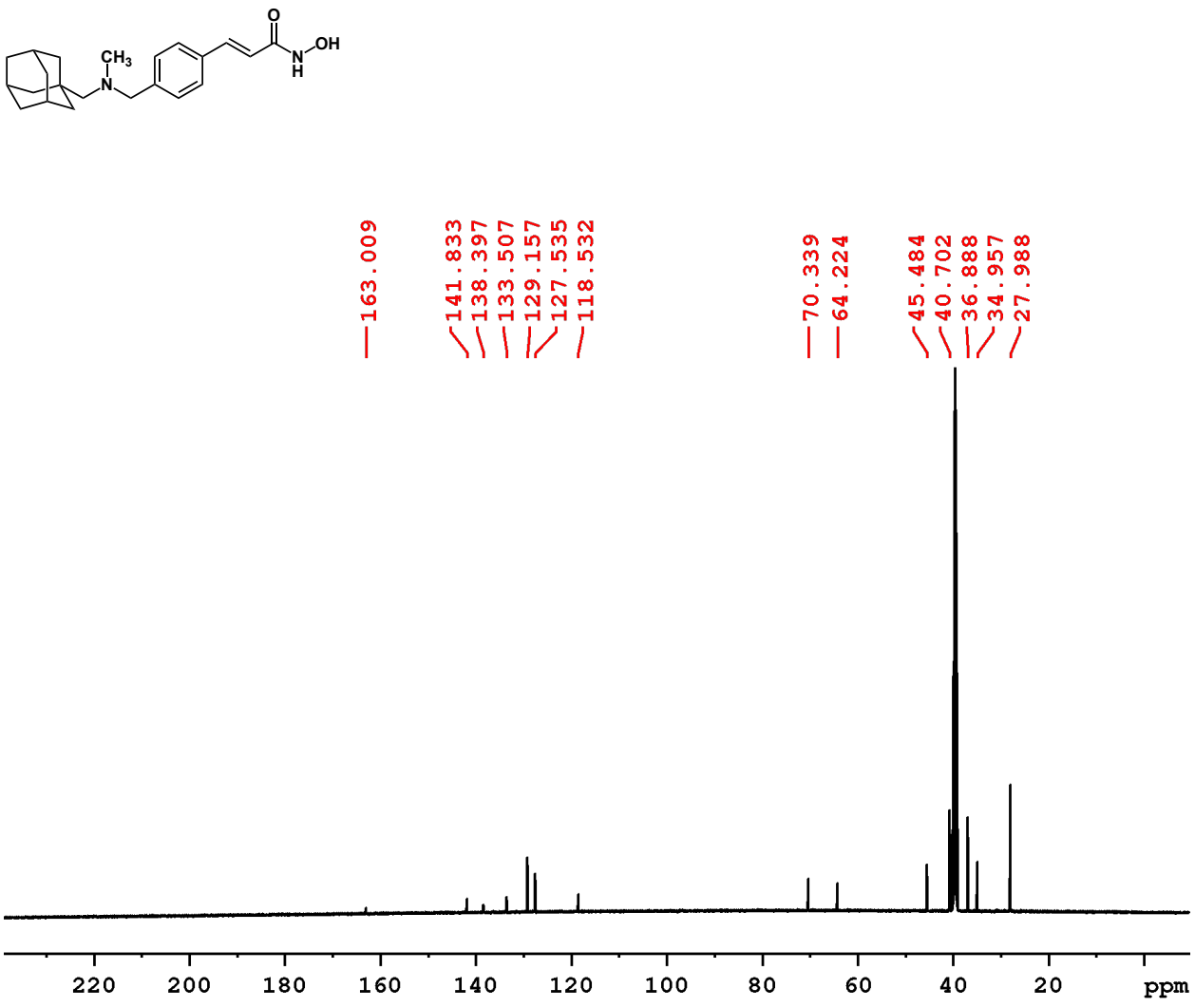

Figure 2-17. $^{13}C\{^{1}H\}$ NMR spectrum of compound 1C in DMSO-d.

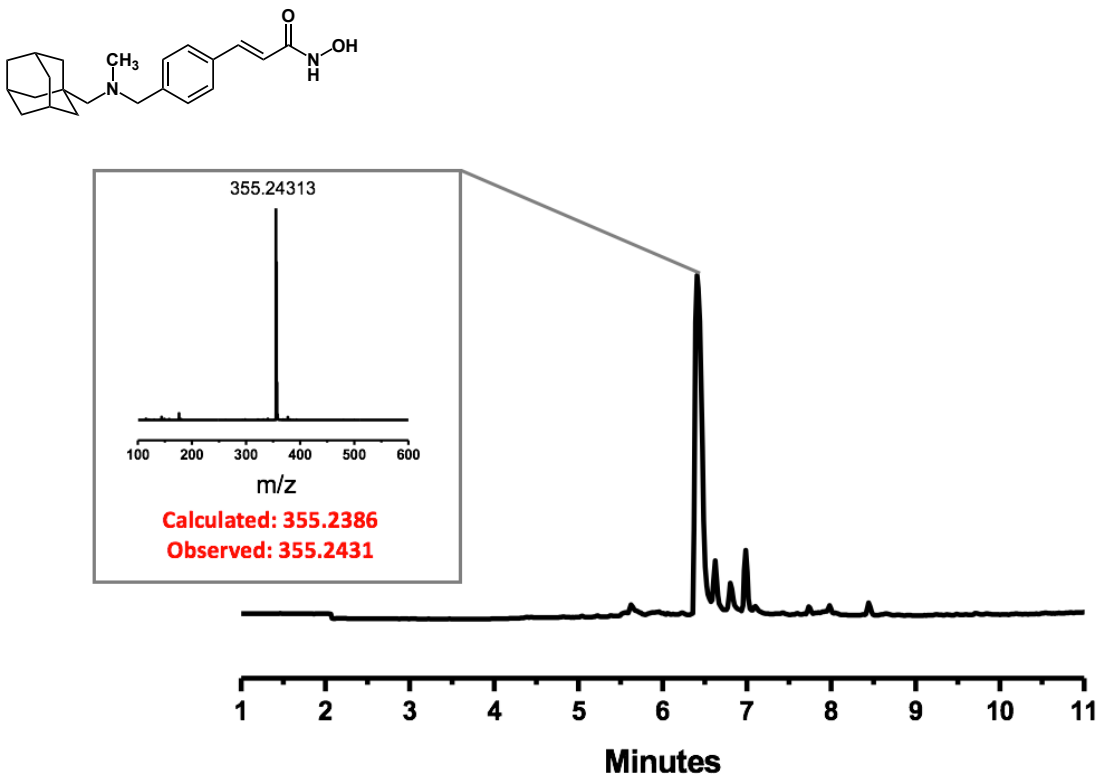

Figure 2-18. LCMS TIC trace for 1C including mass spectrum.

2. 3. 2. Characterization of Carboranostat I

Compound 3A was characterized by ^{1}H (**Figure 2-19**), ^{11}B (**Figure 2-20**), and ^{11}B{H} (**Figure 2-21**) NMR spectroscopy. Compound 3B was also characterized by ^{1}H (**Figure 2-22**), ^{11}B (**Figure 2-23**), and ^{11}B{H} (**Figure 2-24**) NMR spectroscopy, as well as LCMS (**Figure 2-25**). Similarly, 1C was characterized by ^{1}H (**Figure 2-26**), ^{13}C{H} (**Figure 2-27),** ^{11}B (**Figure 2-28**), and ^{11}B{H} (**Figure 2-29**) NMR spectroscopy, as well as LCMS (**Figure 2-30**).

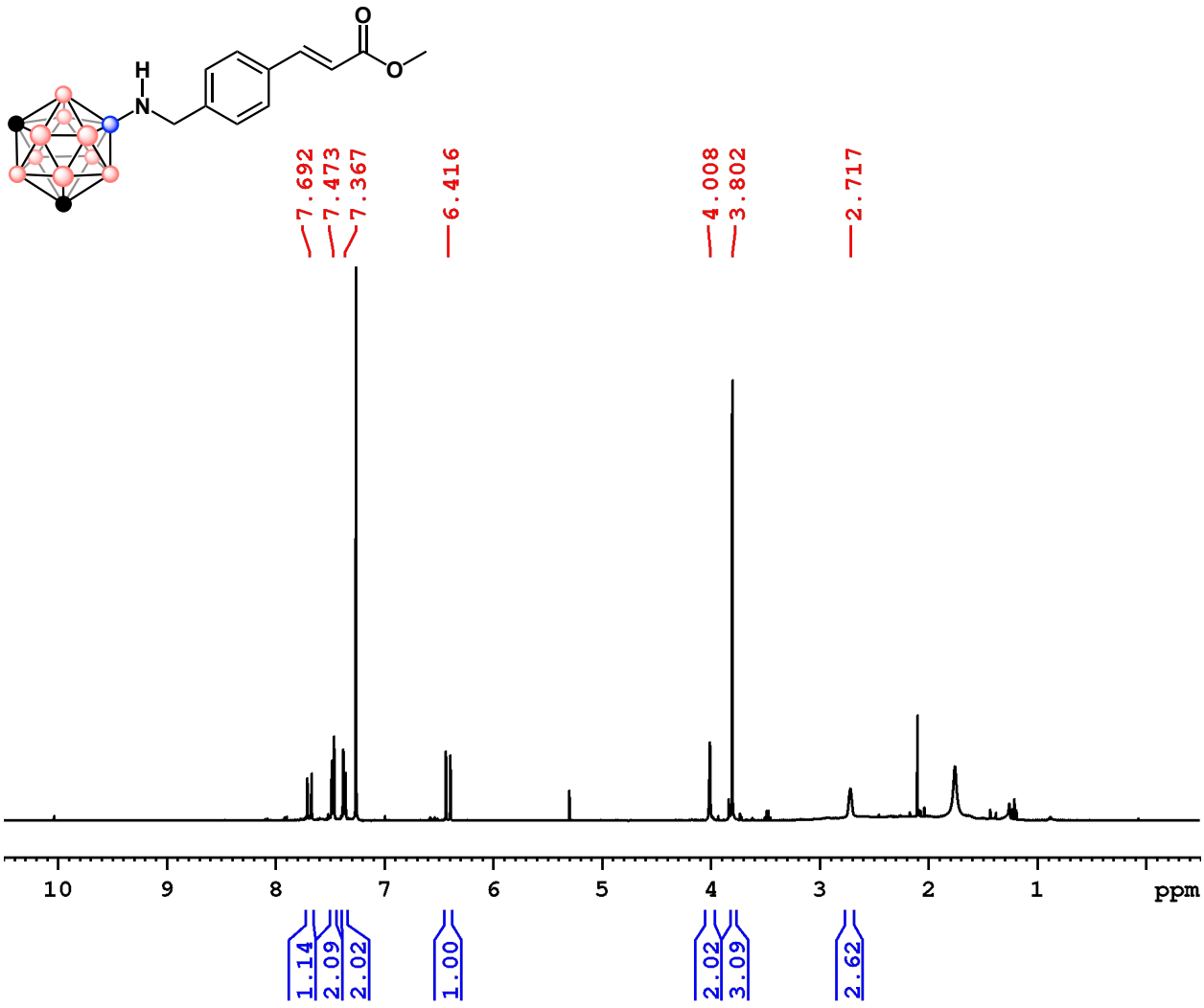

Figure 2-19. ^{1}H NMR spectrum of compound 3A in $CDCl_3$.

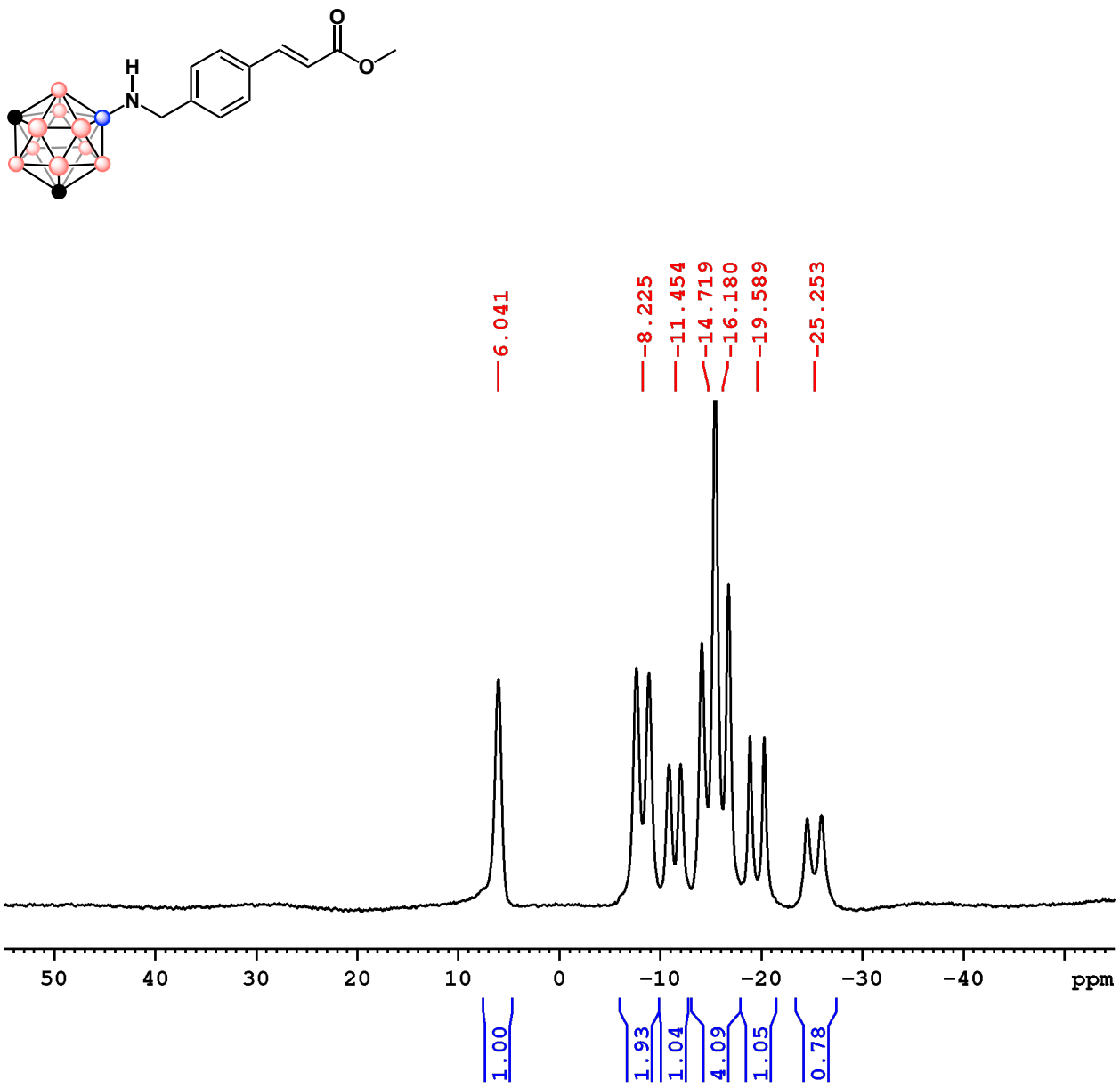

Figure 2-20. ^{11}B NMR spectrum of compound 3A in $CDCl_3$.

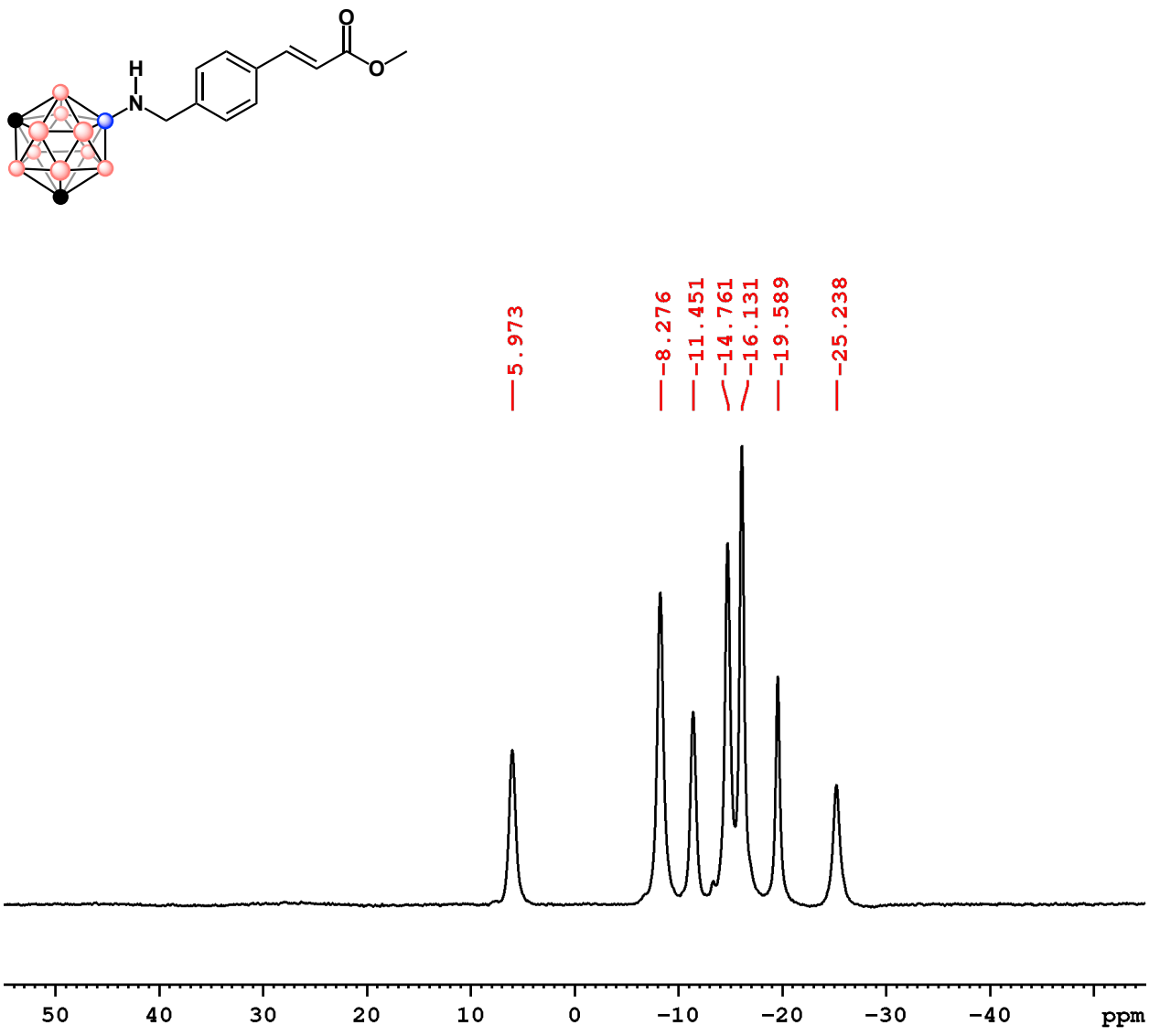

Figure 2-21. $^{11}B\{^{1}H\}$ NMR spectrum of compound 3A in $CDCl_3$.

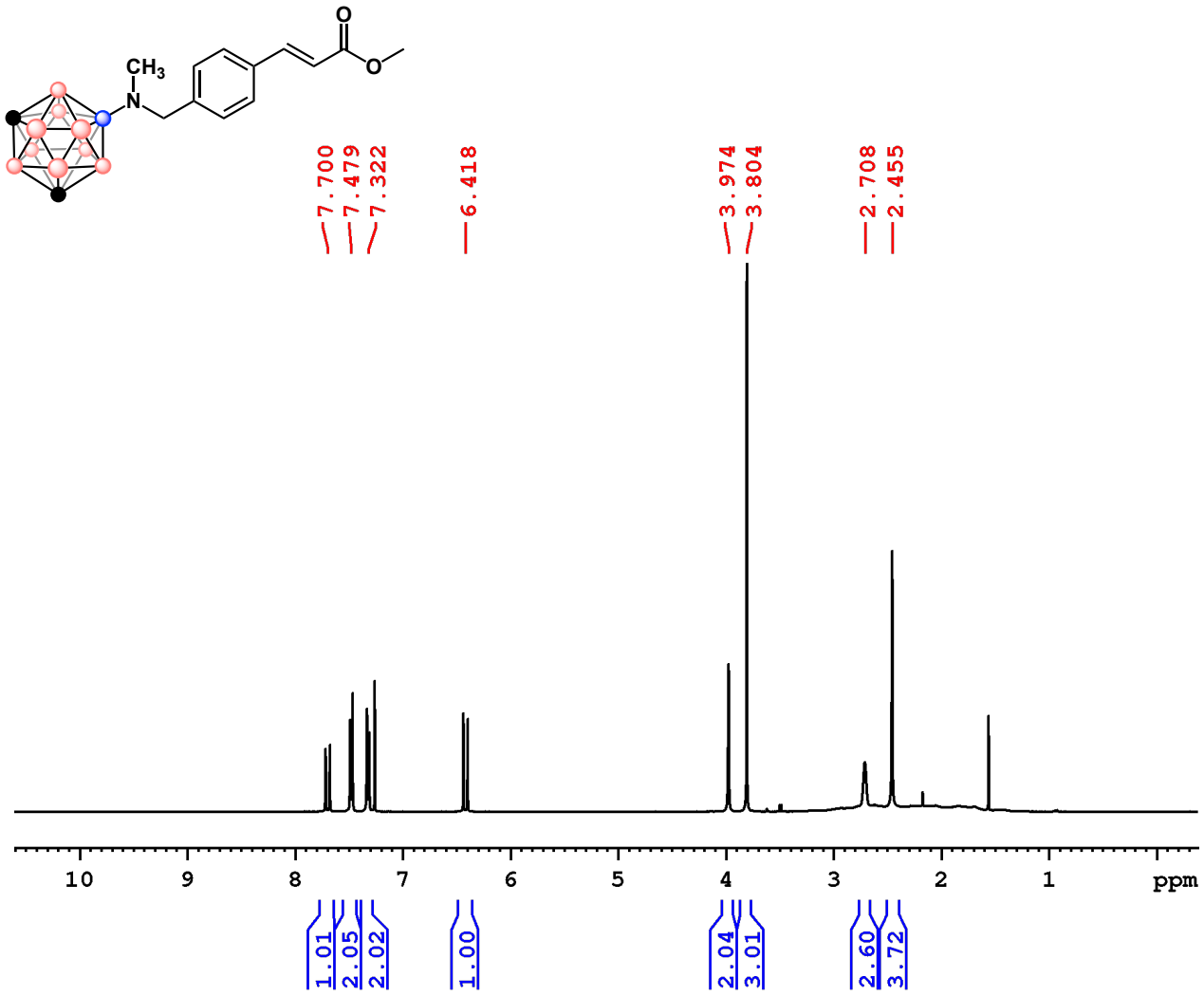

Figure 2-22. ^{1}H NMR spectrum of compound 3B in $CDCl_3$.

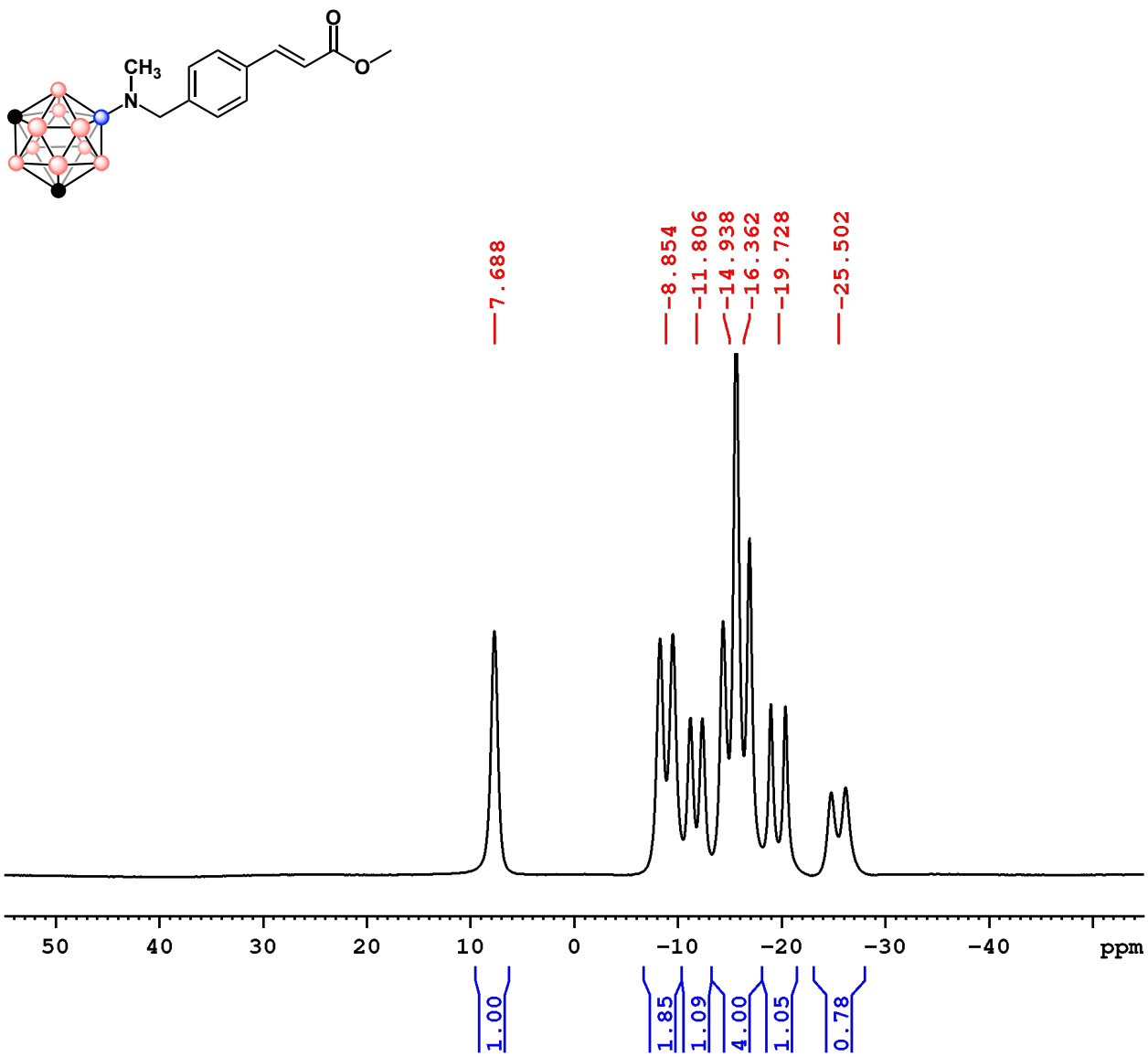

Figure 2-23. ^{11}B NMR spectrum of compound 3B in $CDCl_3$.

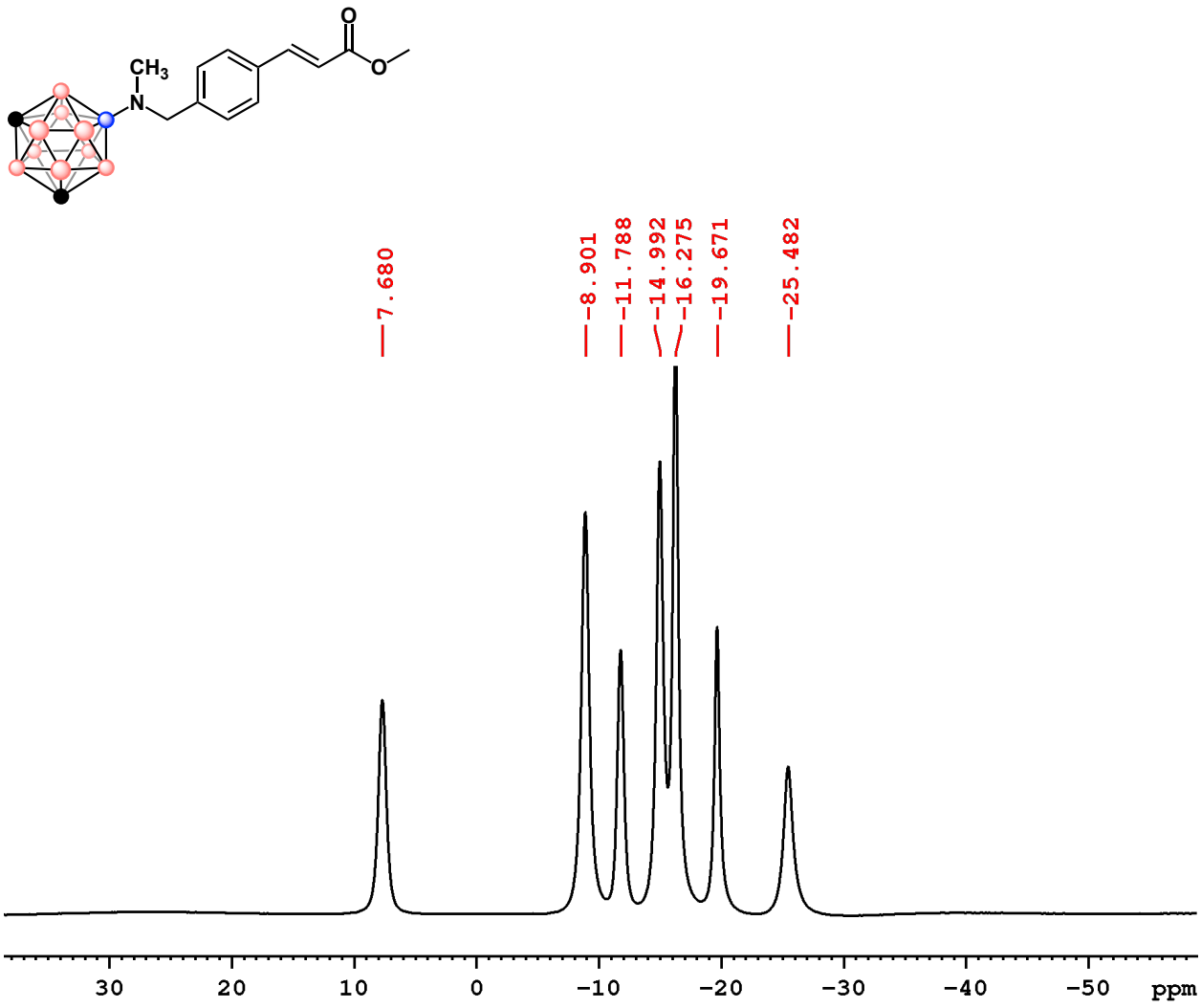

Figure 2-24. $^{11}B\{^{1}H\}$ NMR spectrum of compound 3B in $CDCl_3$.

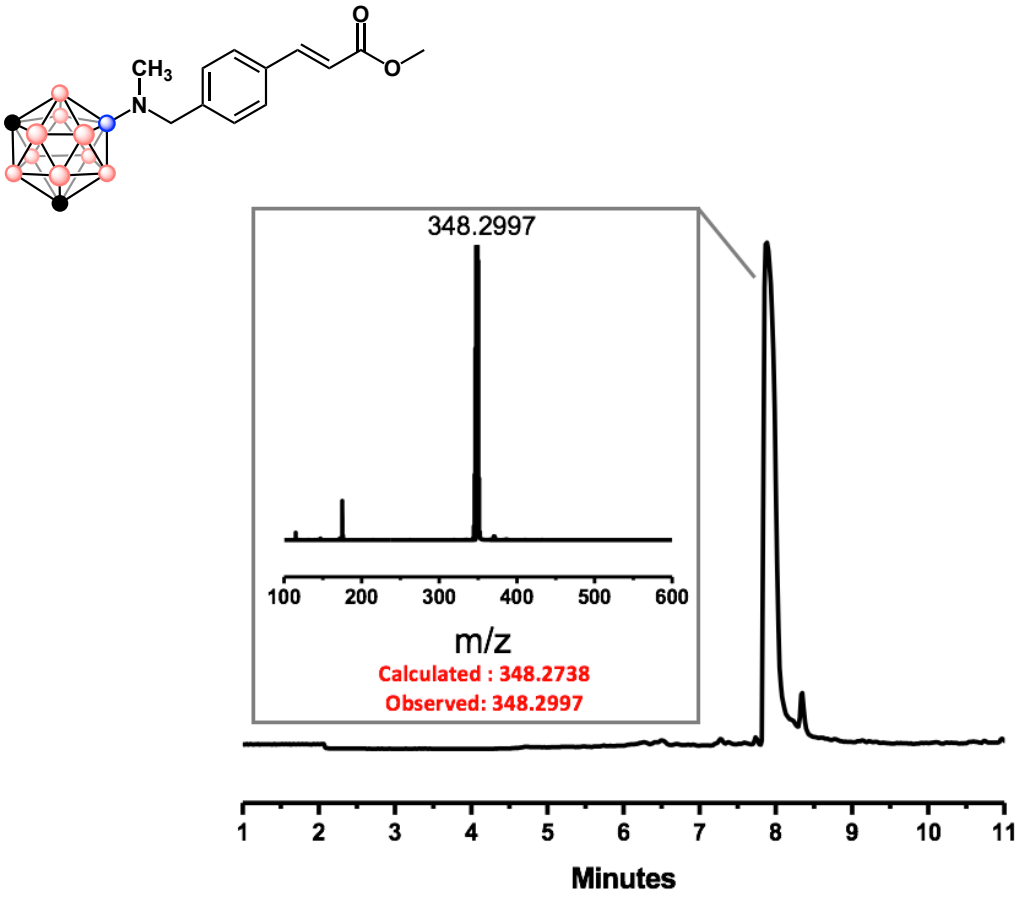

Figure 2-25. LCMS TIC trace for 3B including mass spectrum.

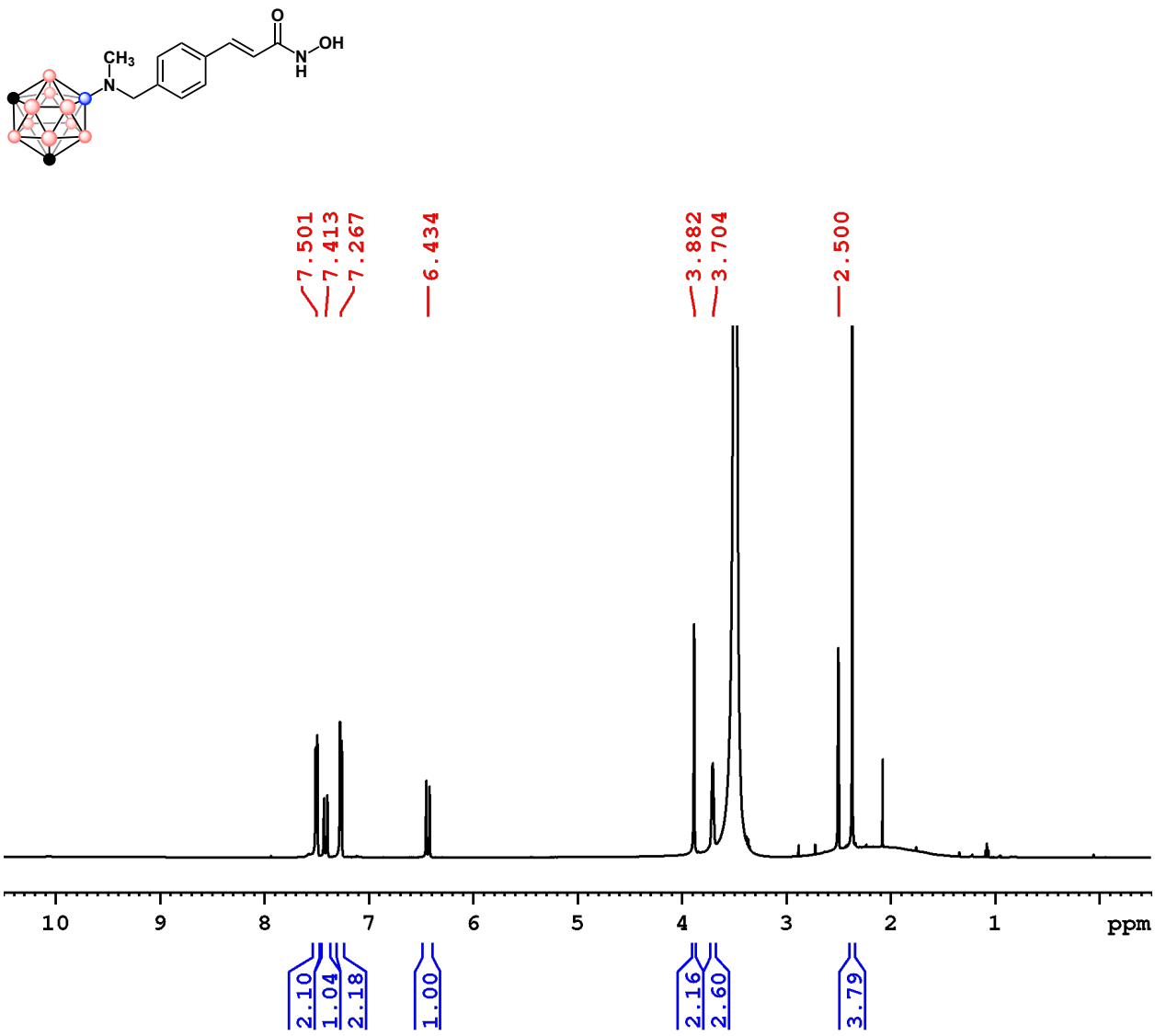

Figure 2-26. ^{1}H NMR spectrum of compound 3C in DMSO-d. Peak at 3.49 is water.

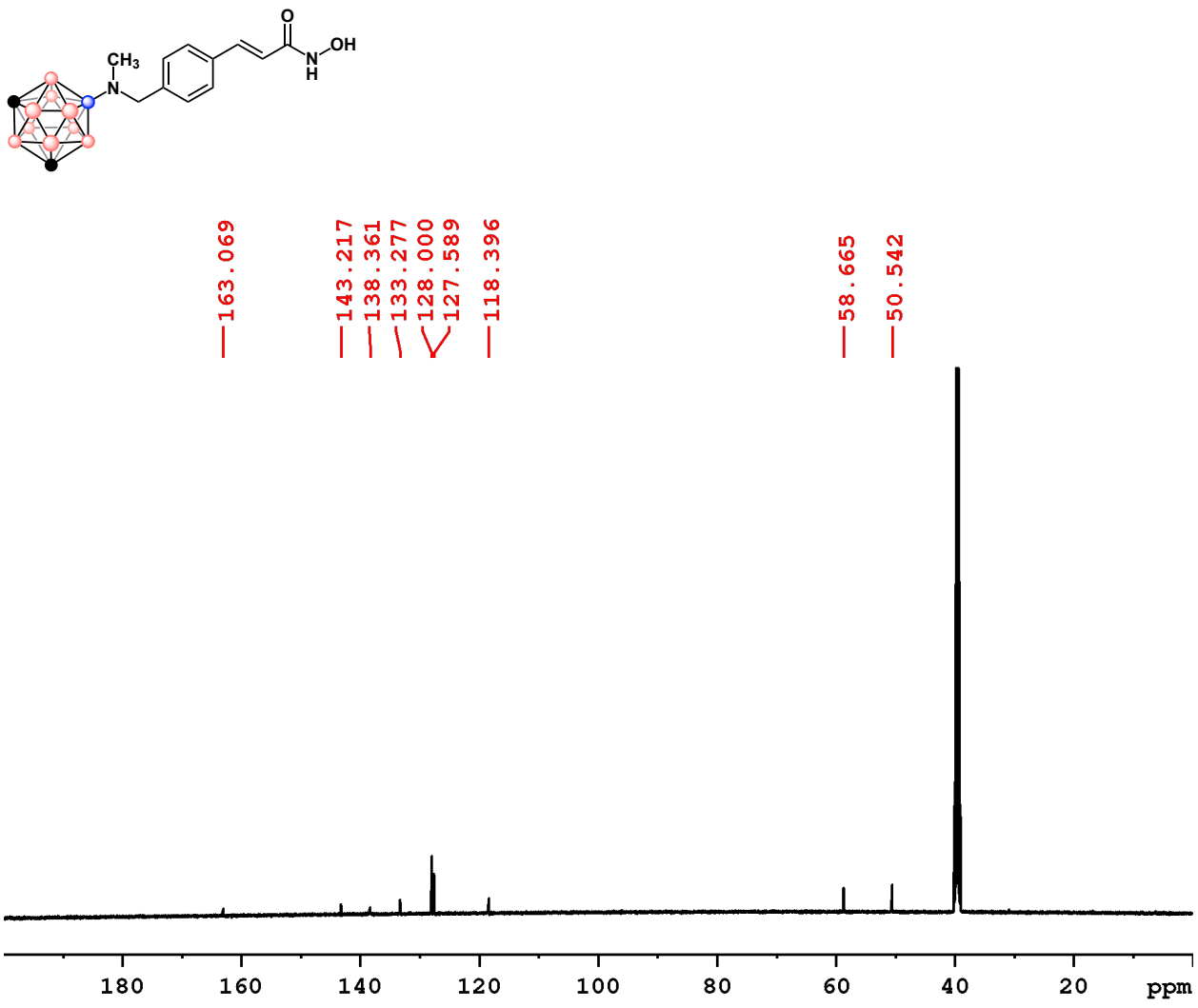

Figure 2-27. $^{13}C\{^{1}H\}$ NMR spectrum of compound 3C in DMSO-d.

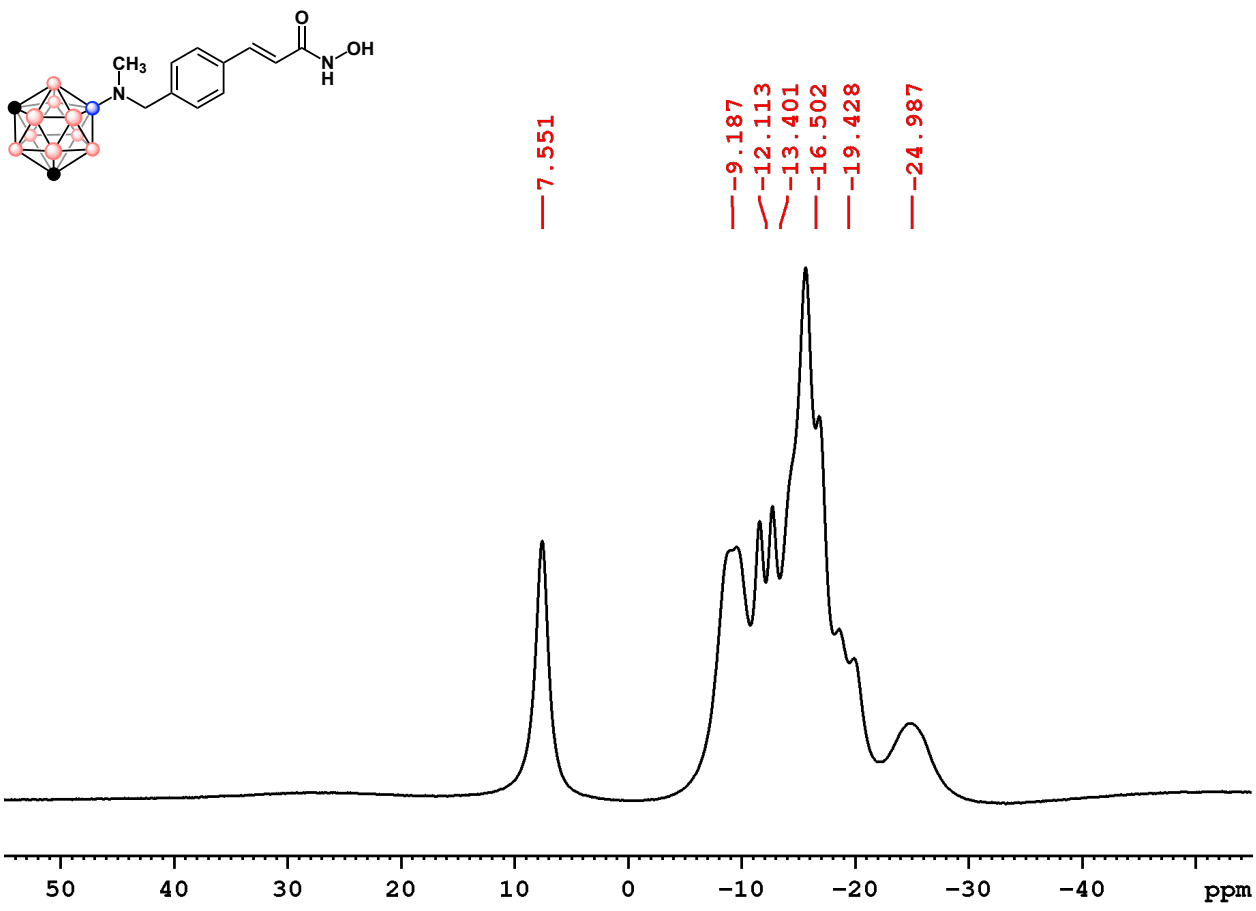

Figure 2-28. ^{11}B NMR spectrum of compound 3C in DMSO-d.

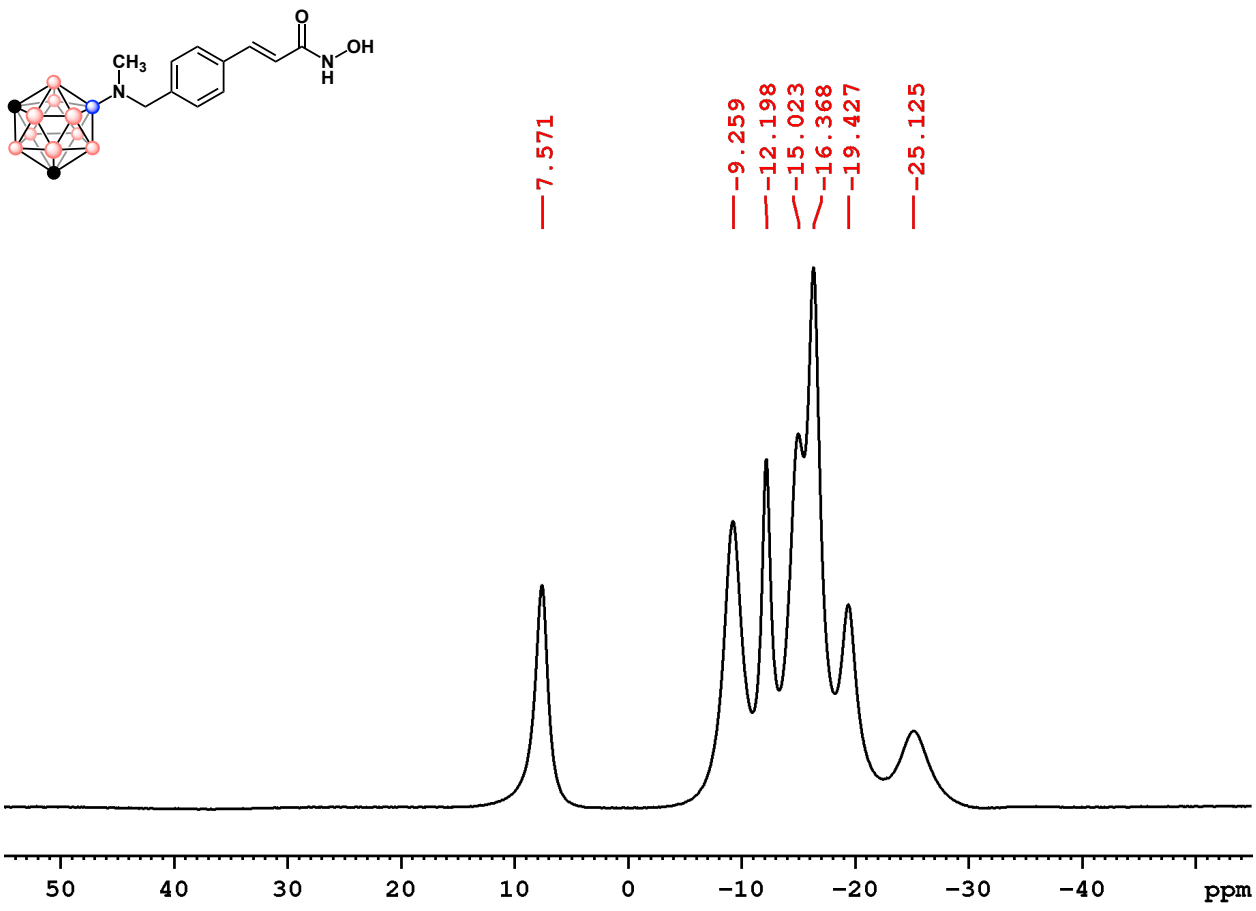

Figure 2-28. $^{11}B\{^{1}H\}$ NMR spectrum of compound 3C in DMSO-d.

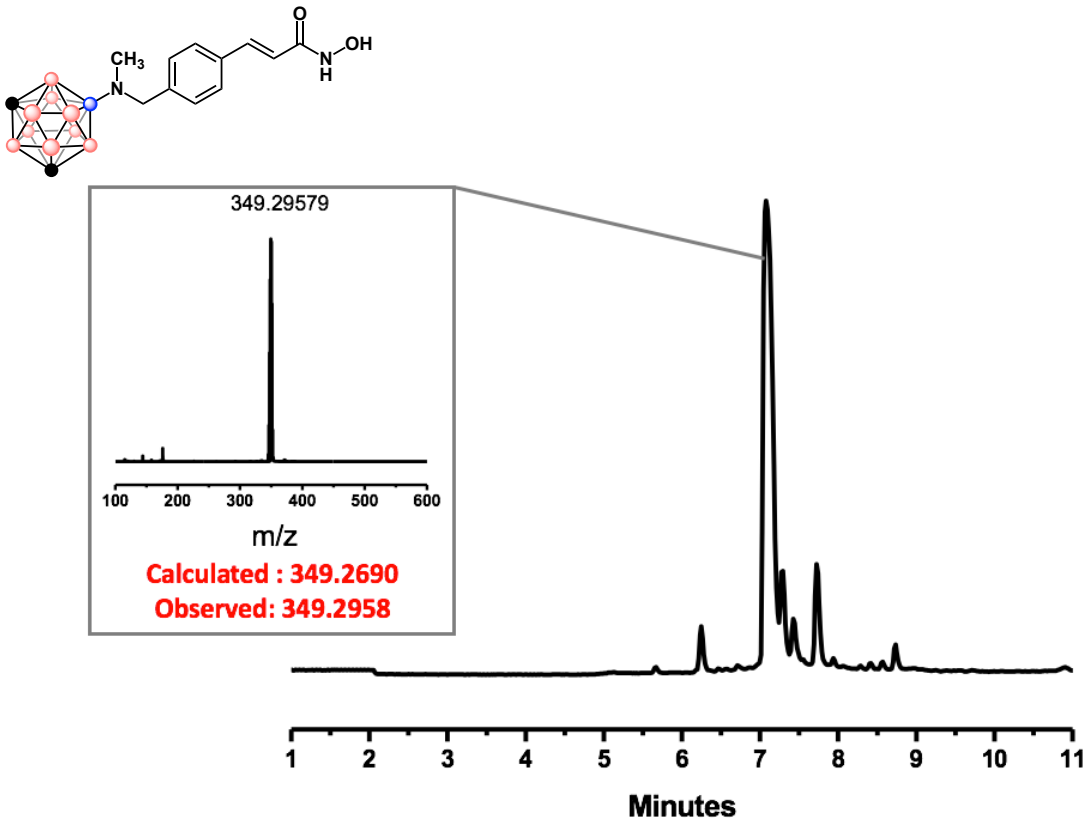

Figure 2-30. LCMS TIC trace for 3C including mass spectrum.

2. 3. 3. HDAC Binding Assay Analysis

The results from the HDAC assay kit are presented in **Figure 2-31**. The blue and orange plots represent inhibition curves for Martinostat and Carboranostat I respectively. According to this data, Carboranostat I is not as effective in inhibition of HDAC2 as Martinostat. Compared to Martinostat, a higher concentration of Carboranostat I is required to cause the same amount of decrease in HDAC2 activity.

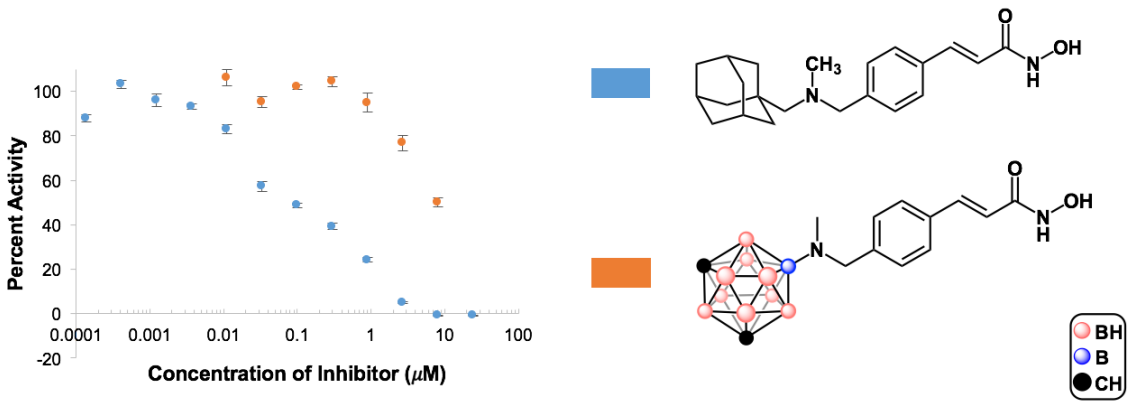

Figure 2-31. Comparison of Martinostat and Carboranostat I in inhibition potency towards HDAC2. On the graph, the percent activity of HDAC2 is depicted as a function of added inhibitor concentration. At 100% activity, no inhibition is observed and at 0% all HDAC activity is seized. Error bars represent standard error of mean (SEM).

2.4. Discussion and Future Steps

The results indicate successful synthesis of Carboranostat I, an HDAC inhibitor analogue featuring a carborane as the cap group. Based on the *in vitro* binding assays, however, Carboranostat I exhibits lower HDAC inhibition activity compared to Martinostat. Reduced potency of Carboranostat I could perhaps be due to lack of a full chemical analogy between the two molecules. The structure of Martinostat incorporates a methylene group (-CH_2) between the cap group—adamantane in this case—and the amine group on the linker. This methylene group is absent in the structure of Carboranostat I. This additional "spacer" group may be critical in granting adequate flexibility to the cap group and facilitating stronger binding. In order to investigate this hypothesis, we intend to synthesize another analogue, which incorporates the spacer group between carborane cap group and the linker (**Figure 2-32**).

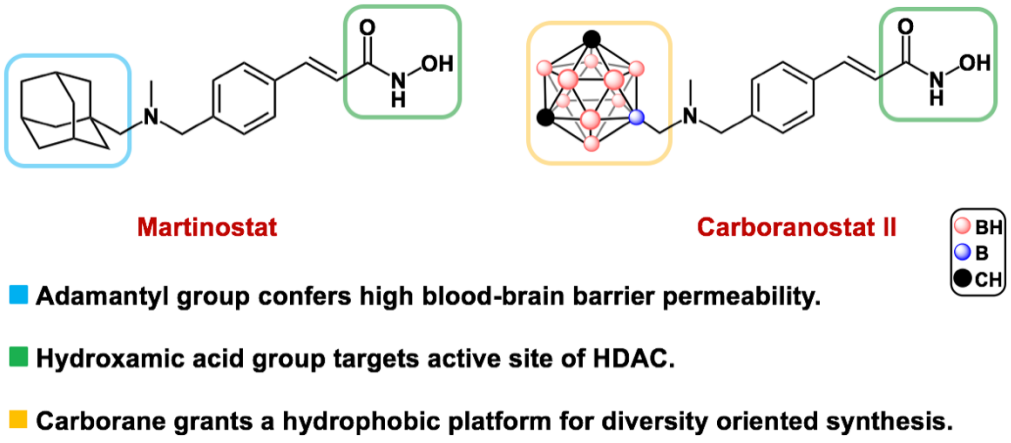

Figure 2-32. The structure of the new synthetic target, Carboranostat II, is depicted. Carboranostat II has a methylene spacer between the bulky cap group and the amine on the linker, as is the case with Martinostat. It is hypothesized that this spacer group would increase the flexibility of the cap group and lead to effective HDAC inhibition.

2.5. References

1. Grunstein, M. *Nature*, **1997**, 389, 349-352.
2. Jenuwein, T., and Allis, C. D. *Science*, **2001**, 293, 1074-1080.
3. Strahl, B. D., and Allis, C. D. *Nature*, **2000**, 403, 41-45.
4. Lombardi, P. M., Cole, K. E., Dowling, D. P., and Christianson, D. W. *Curr Opin. Struct. Biol.*, **2011**, 21, 735-743.
5. Marks, P. A., Rifkind, R. A., Richon, V. M., Breslow, R., Miller, T., and Kelly W. K. *Nat. Rev. Cancer*, **2001**, 1, 194-202.
6. Cress, W. D., and Seto, E. *J. Cell. Physiol.*, **2000**, 184, 1-16.
7. Kilgore, M., Miller, C. A., Fass, D. M., Hennig, K. M., Haggarty, S. J., Sweatt, J. D., and Rumbaugh, G. *Neuropsychopharmacology*, **2010**, 35, 870-880.
8. Kazantsev, A. G., and Thompson, L. M. *Nat. Rev. Drug Discov.*, **2008**, 7, 854-868.
9. Kennedy, P. J., Feng, J., Robison, A. J., Maze, I., Badimon, A., Mouzon, E., Chaudhury, D., Damez-Werno, D. M., Haggarty, S. J., Han, M. H., Bassel-Duby, R., Olson, E. N., and Nestler, E.J. *Nat. Neurosci.*, **2013**, 16, 434-440.
10. Malvaez, M., McQuown, S. C., Rogge, G. A., Astarabadi, M., Jacques, V., Carreiro, S., Rusche, J. R., and Wood, M. A. *Proc. Natl. Acad. Sci. U. S. A.*, **2013**, 110, 2647-2652.
11. Robinson, A. J., and Nestler, E. J. *Nat. Rev. Neurosci.*, **2012**, 12, 623-637.
12. Kennedy, P. J., and Harvey, E. *CNS Neurol. Disord. Drug Targets*, **2015**, 14, 764-772.
13. Hooker, J. M., Kim, S. W., Alexoff, D., Xu, Y., Shea, C., Reid, A., Volkow, N., and Fowler, J. S. *ACS Chem. Neurosci.*, **2010**, 1, 65-73.
14. Dokmanovic, M., Clarke, C., and Marks, P. A. *Mol. Cancer Res.*, **2007**, 5, 981-989.
15. Bieliauskas, A. V., and Pflum M. K. H., *Chem. Soc. Rev.*, **2008**, 37, 1402-1413.

16. Falkenberg, K. J., and Johnstone, R. W. *Nat. Rev. Drug Discov.*, **2014**, 13, 673-691.

17. Lee, J. H., Mahendran, A., Yao, Y., Ngo, L., Venta-Perez, G., Choy, M. L., Kim, N., Ham, W. S., Breslow, R., and Marks, P. A. *Proc. Natl. Acad. Sci. U. S. A.*, **2013**, 110, 15704-15709.

18. Shao, W., Growney, J. D., Feng, Y., O'Connor, G., Pu, M., Zhu, W., Yao, Y. M., Kwon, P., Fawell, S., and Atadja, P. *Int. J. Cancer.*, **2010**, 127, 2199-2208.

19. Wang, C., Schroeder, F. A., Wey, H. Y., Borra, R., Wagner, F. F., Reis, S., Kim, S. W., Holson, E. B., Haggarty, S. J., and Hooker, J. M. *J. Med. Chem.*, **2014**, 57, 7999–8009.

20. Schroeder, F. A., Wang, C., Van de Bittner, G. C., Neelamegam, R., Takakura, W. R., Karunakaran, A., Wey, H. Y., Reis, S. A., Gale, J., Zhang, Y. L., Holson, E. B., Haggarty, S. J., and Hooker, J. M. *ACS Chem. Neurosci.*, **2014**, 5, 1055-1062.

21. Wey, H. Y., Wang, C, Schroeder, F. A., Logan, J., Price, J. C., Hooker, J. M. *ACS Chem. Neurosci.*, **2015**, 6, 708-715.

22. Spokoyny, A. M. *Pure Appl. Chem.*, **2013**, 85, 903-919.

23. Kracke, G. R., VanGordon, M. R., Sevryugina, Y. V., Kueffer, P. J., Kabytaev, K., Jalisatgi, S. S., and Hawthorne, M. F. *ChemMedChem.*, **2015**, 10, 62-67.

24. Schwartz, J. J., Mendoza, M. A., Wattanatorn, N., Zhao, Y., Nguyen, V. T., Spokoyny, A. M., Mirkin, C. A., Baše, T., and Weiss, P. S. *J. Am. Chem. Soc.*, **2016**, 138, 5957-5967.

25. Issa, F., Kassiou, M., and Rendina, L. M. *Chem. Rev.*, **2011**, 111,5701-5722.

26. Plešek, j. *Chem. Rev.*, **1992**, 92, 269-278.

27. Dziedzic, R. M., Saleh, L. M. A., Axtell, J. C., Martin, J. L., Stevens, S. L., Royappa, A. T., Rheingold, A. L., and Spokoyny, A. M. *J. Am. Chem. Soc.*, **2016**, 138, 9081-9084.

28. Dziedzic, R. M., Martin, J. L., Axtell, J. C., Saleh, L., Ong, T.-C., Yang, Y.-F., Messina, M. S., Rheingold, A. L., Houk, K. N., and Spokoyny, A. M. *J. Am. Chem. Soc.*, **2017**, 139, 7729-7732.

29. Zhdanko, A., Schmauder, A., Ma, C. I., Sibley, L. D., Sept, D., Sasse, F., and Maier, M. E. *Chemistry*, **2011**, 17, 13349-13357.